Chapter 2

Effect of salt stress and varying cultivation strategies on bioenergy feedstock production in *Chlamydomonas reinhardtii*

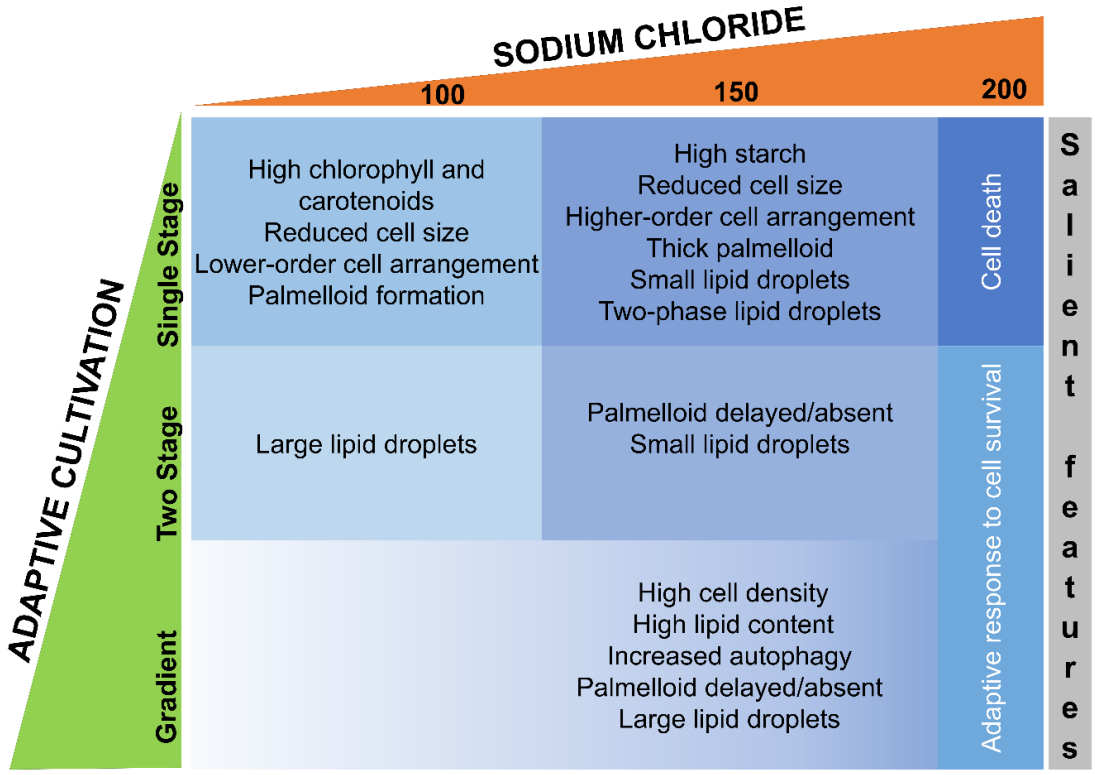

2 Effect of salt stress and varying cultivation strategies on bioenergy feedstock production in *Chlamydomonas reinhardtii*

2.1 Abstract

High salt concentrations cause osmotic shock and oxidative imbalance in the microalgal cell, thereby causing cell death, yet salt stress is very effective in increasing bioenergy feedstock production. Thus, innovative strategies are required to overcome the survival barrier and enhance the net productivity of bioenergy feedstock like starch, carotenoids, and lipids. In the current study, a gradient strategy for salt addition was employed to cultivate *Chlamydomonas reinhardtii*, and the effect of the step size was also analyzed. It was found that 100 mM NaCl does not hamper cell growth and benefits the net yield of chlorophyll and carotenoids, resulting in the highest production as compared to the Control. Gradient and two-stage methods increased the survival rate of microalgal cells at 200 mM NaCl. The highest production of starch and lipids was obtained at 150 mM NaCl, from single-stage and gradient methods, respectively. Starch production preceded lipid synthesis in the growth cycle. The combined action of autophagy, *de novo* lipid synthesis, and starch degradation together were found to enhance the triacylglycerol production in the gradient method. Salinity stress was observed to induce the palmelloid formation, with the cell wall enclosing a gel matrix containing 6 or more cells in single-stage growth, otherwise absent or delayed in two-stage and gradient. The cell size and shape in the gradient method remain unchanged. The single stage produces smaller-sized lipid droplets while the gradient induces the assembly of larger droplets. The lipid droplet growth dynamics were found to lead to the liquid-liquid phase separation of lipid droplets from the cytosol. The existence of phase separation was shown to be dependent on the mode of cultivation and age of the culture. Overall, the gradient-strategy approach led to increasing biofuel productivity and metabolite production. The findings of this study unveil the basic knowledge of lipid droplet assembly which could be used for large-scale lipid production.

2.2 Introduction

Salt stress is a well-studied cultivation environment to enhance the biofuel potential of microalgae (Bazzani et al., 2021). Marine microalgal strain, *Chlamydomonas* sp. JSC4 generated high lipid content under nitrogen-depleting hypersaline conditions (Ho et al., 2014). *Chlamydomonas reinhardtii* showed a dramatic increase in the fatty acid content in presence of different salts like NaCl, KCl, and LiCl (Atikij et al., 2019). Fan *et al*. show that 0-50 mM NaCl results in efficient photosynthesis in *C. reinhardtii*, but is negatively affected by 100- 200 mM NaCl (Fan and Zheng, 2017). NaCl at 200 mM resulted in cell death, while at 100 mM *Chlamydomonas* cells show deteriorating growth and maximum lipid content is obtained at 50 mM NaCl (Salama et al., 2013; Fan and Zheng, 2017). Increased salinity imposes an osmotic shock on microalgal cells, causing cell size reduction and the formation of palmelloids for protection (Bazzani et al., 2021). Carbon partitioning and starch-to-lipid switching are essential contributors to the enhanced lipid content observed under high salinity (Zhang et al., 2018; Ho et al., 2017). Intracellularly, it also results in oxidative stress and high ROS levels further activate autophagy-driven lipid accumulation (Fal et al., 2022). However, prolonged exposure to high ROS levels is often fatal for photosynthesis and cell growth (Fal et al., 2022). Carotenoids can quench the ROS molecules and prevent cell damage (Pérez-Pérez et al., 2012).

Studies have shown that liquid-liquid phase separation of lipid droplets (LD) is involved in maintaining cellular redox levels (Saito and Kimura, 2021). Liquid-liquid phase separation is also a well-known phenomenon involved in regulating lipid droplet formation under stress (Zoni et al., 2020). Lipid droplet formation acts as a buffer to protect the cell from free fatty acid toxicity during stress (Olzmann and Carvalho, 2019). Lipid droplets are stabilized in the cytosol due to the presence of a phospholipid monolayer at the interface, which decreases the interfacial surface tension and enhances the bending rigidity (Chernomordik and Kozlov, 2003; Thiam et al., 2013; Georgieva et al., 2009). Despite the acquired metastability, LD can increase in size due to Ostwald ripening and droplet coalescence (Walther et al., 2017). Lipids like triacylglycerols, have minimal solubility in aqueous media and hence have decreased Ostwald ripening processes. Droplet coalescence initiates with the development of a transient pore formation between the coalescing droplets spatially close to each other, eventually leading to the complete fusion of the droplets (Walther et al., 2017; Georgieva et al.,

2009). The pore formation depends on the elasticity of the phospholipid monolayer at the interface, as the bending rigidity of this layer defines the energy cost required to deform this surface, which can be quantified by the line tension, Γ. The thermal fluctuations also drive the transient pore formation, and droplet coalescence occurs if the energy barrier given by Γ^2/γ is overcome. If surface tension γ is high and line tension, Γ is low, the energy barrier is less, then droplet coalescence becomes more probable (Thiam and Forêt, 2016). Hence the lipid droplets present a dynamically changing scenario and depend on the lipid turnover, droplet concentration fluctuations, enhanced lipid synthesis, and droplet growth by Oswald ripening and/or fusion (Yu and Li, 2017). It would be interesting to study the droplet growth dynamics in microalgae when exposed to salt stress.

Salt stress results in the loss of lipid productivity due to cell death and poor biomass (Bazzani et al., 2021). Two-stage cultivation has been found to cause biomass accumulation in the first stage, followed by exposure to stress elements in the second stage. This was observed to increase the net content of the lipid content in microalgae (Nagappan et al., 2019). Two-stage salt stress in *Chlamydomonas* sp. JSC4 has been observed to increase biomass accumulation and lipid content by nearly four times compared to single-stage (Ho et al., 2014). In *Scenedesmus* sp. CCNM 1077, supplementing 400 mM NaCl in the second stage is observed to reduce the detrimental effects of stress and increases the production of biomass, chlorophylls, and carotenoids by as high as three times compared to single-stage cultivation (Pancha et al., 2015). A significant increase in lipid content by 2.5 times was also observed in *Chlorella vulgaris* when 500 mM NaCl was added with a two-stage strategy (Yun et al., 2019). Recently, an advanced approach has evolved where stress elements are introduced in a stepwise/gradient strategy to induce gradual adaptation to stress (Maneechote and Cheirsilp, 2021). Ho et al. (2014) experimented with marine microalga, *Chlamydomonas* sp. JSC4 using salt stress combined with nitrogen depletion. The authors observed maximum lipid content and lipid productivity in the case of salinity gradient. In a separate study, salinity-gradient in *Chlamydomonas* sp. JSC4 also resulted in enhanced biomass and lutein production (Xie et al., 2019). Salinity gradient in other microalgae also results in improved biofuel potential (Zhang et al., 2017; Gour et al., 2020). However, the possible alterations in the microalgal morphology and the

metabolic pathways responsible for the enhanced biofuel potential in two-stage and salinity gradient cultivation remains to be identified.

In this study, the effect of NaCl at different concentrations applied in single-stage, two-stage, and gradient to *Chlamydomonas reinhardtii* CC-125 is explored. The production of energy-rich compounds, i.e., starch and lipids, and photosynthetic pigments, i.e., chlorophyll and carotenoids are studied as the function of culture age and growth phase. Using qRT-PCR, the role of genes involved in autophagy, starch-to-lipid switching, and *de novo* lipid synthesis was investigated in two-stage and gradient modes of cultivation. Interestingly, bifurcated distribution of functions was observed in single-stage *versus* gradient. Lastly, single-cell fluorescence microscopy was performed to study the lipid droplet distribution and the morphological changes induced upon exposure to salt stress in different modes of cultivation. This study shows the involvement of liquid-liquid phase separation in lipid droplet formation in microalgae exposed to salt stress. Overall, the current work encompasses many aspects of *C. reinhardtii* grown in salt stress unraveling both the phenotypic and genotypic changes it undergoes that result in enhanced bioenergy feedstock production.

2.3 Materials and Methods

2.3.1 Growth and maintenance of *Chlamydomonas reinhardtii* CC-125

Chlamydomonas reinhardtii CC-125 used throughout this study, was procured from Chlamydomonas Resource Centre, Minnesota, USA. Microalgal cells were grown and maintained on Tris-acetate-phosphate (TAP) medium pH 7.0 (see Appendix A1 for composition), containing 40 µg/mL ampicillin. The culture was grown at 25 °C with constant shaking at 200 rpm, and white light of ~50 µmol photons m^{-2} s^{-1} was provided maintaining a light: dark cycle of 12h: 12h light.

2.3.2 Cultivation strategies of *C. reinhardtii* under salt stress

Salt stress was provided using sodium chloride (NaCl) at three different concentrations, 100 mM, 150 mM, and 200 mM. In the single-stage mode of cultivation, (designated as SS_100, SS_150, and SS_200), salt was added at the commencement of cultivation for each concentration. In the two-stage (designated as D*x*_100, D*x*_150, and D*x*_200),

salt was added on the x^{th} day of growth. In this study, x = 2 or 4, i.e., in the log phase of the culture. In the gradient mode of cultivation, a known concentration of salt is added stepwise at fixed time intervals to achieve the final concentration. Gradient strategy is applied only for 150 mM and 200 mM NaCl concentrations, which are categorized into two types: g15_10_150 and g20_10_200 have 15 mM and 20 mM NaCl, added daily respectively, up to 10 days of growth, while g30_10_150 and g40_10_200 have doubled the NaCl concentration, i.e., 30 mM and 40 mM, respectively, added on alternate days up to 10^{th} day of growth. Thus, the final concentration in both cases is attained at the same time of growth but in varying step sizes, it is 1 day in the first case and 2 days in the latter. The schematic representation of salt stress delivered for the final concentration of 100 mM is illustrated in **Figure 2.1**. A similar representation for the 150 mM and 200 mM NaCl concentrations is made in **Figure 2.2**.

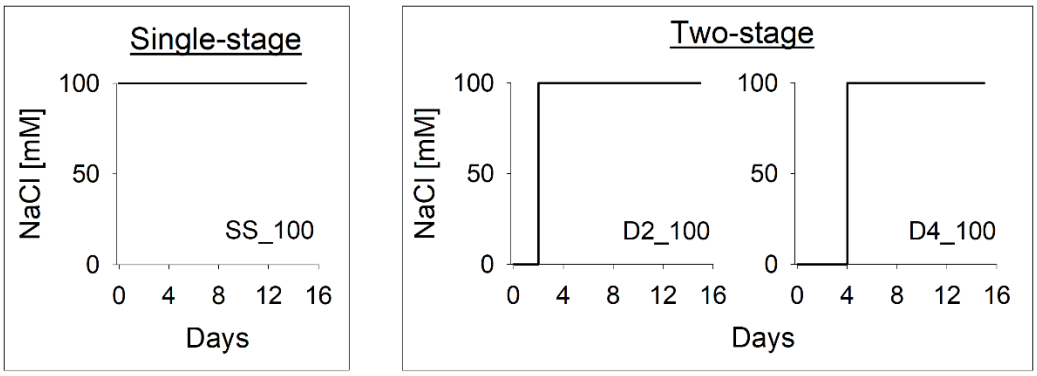

Figure 2.1. A schematic representation of salt stress addition in single-stage and two-stage methods of cultivation to achieve the final concentration of 100 mM NaCl.

Here, SS_100 represents a single stage. In D2_100, 100 mM NaCl is added on the 2^{nd} day of cultivation, and in D4_100, 100 mM NaCl is added on the 4^{th} day of cultivation.

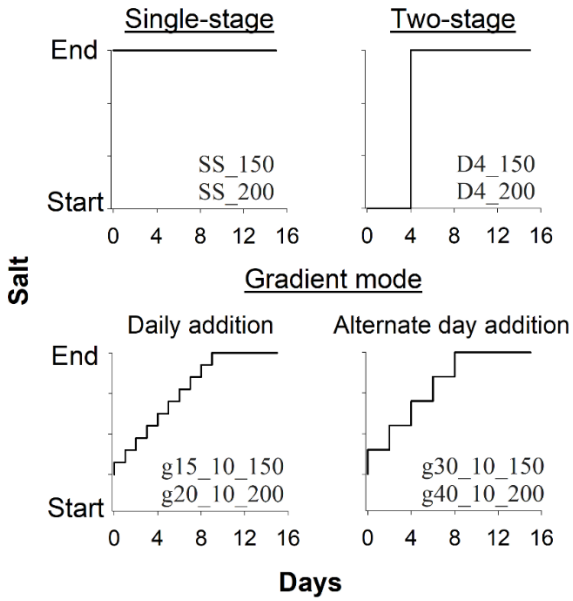

Figure 2.2. A schematic representation of single-stage, two-stage, and gradient strategy of cultivation in presence of 150 mM and 200 mM NaCl.

Here, D4_150 and D4_200 mean the respective amount of NaCl is added on the 4th day of cultivation. g15_10_150 and g20_10_200 have 15 mM and 20 mM NaCl, respectively, added daily for up to 10 days of growth. The step size here is 1 day. g30_10_150 and g40_10_200 have doubled the NaCl concentration, i.e., 30 mM and 40 mM, respectively, added on alternate days up to the 10th day of growth. The step size, thus, is 2 days in this case.

2.3.3 Cell count using a haematocytometer

To avoid redundancy in counting, *Chlamydomonas* cells were first immobilized by providing a 10 min cold shock at 4°C to the liquid culture. The cell count present in a given volume of culture at different growth stages with known absorbance at 680 nm (OD_{680}) was obtained using a haematocytometer and a linear graph between OD_{680} (measured using a UV-Visible spectrophotometer UV-1800, Shimadzu) and the cell count was plotted. An equation correlating cell density and OD_{680} was derived from the linear fit using OriginPro 9.0 software. This equation was used to calculate the cell density directly from measured OD_{680} values.

2.3.4 Analysis of total photosynthetic pigments

Chlamydomonas reinhardtii CC-125 is a green photosynthetic microalga and produces chlorophyll *a* and *b* as the main photosynthetic pigments. Carotenoids are also produced during photosynthesis, where they work as anti-oxidants as well apart from harvesting light. These pigments were extracted in ethanol. In this study, CC-125 cells were

harvested at definite time intervals and resuspended in 95 % ethanol. Pigments solubilized in ethanol were separated from cell debris by centrifugation at 12,000 x g for 5 min. The solubilized pigments were measured using a UV-Vis Spectrophotometer at 664 nm and 648 nm for chlorophylls and 470 nm for carotenoids. The absorbance values were used to calculate the total pigment concentration in mg/mL and mg/10^6 cells, based on the equations given below (**Equations 2.1 to 2.6**) (Khan and Mitchell, 1987).

$$Chl\ a = 13.3OD_{664} - 5.19OD_{648}$$

Equation 2.1 The equation for estimating Chlorophyll *a*

$$Chl\ b = 27.43OD_{648} - 8.12OD_{664}$$

Equation 2.2. The equation for estimating Chlorophyll *b*

$$Chl\ a + b\ \left(\frac{mg}{mL}\right) = 5.24OD_{664} + 22.24OD_{648}$$

Equation 2.3. The equation to calculate total chlorophyll in mg/mL

$$Chl\ a + b\ (mg/10^6\ cells) = \frac{(5.24OD_{664} + 22.24OD_{648})}{Total\ cell\ density} \times 10^6$$

Equation 2.4. The equation for estimating total chlorophyll in mg/10^6 cells

$$Total\ carotenoids\ (mg/mL) = \frac{(1000OD_{470} - 2.13Chl\ a - 97.64Chl\ b)}{209}$$

Equation 2.5. The equation for total carotenoid estimation in mg/mL

$$Total\ carotenoids\ \left(\frac{mg}{10^6}cells\right) = \frac{(1000OD_{470} - 2.13Chl\ a - 97.64Chl\ b)\ /\ 209)}{Total\ cell\ density} \times 10^6$$

Equation 2.6. The equation for estimating total carotenoids in mg/10^6 cells

2.3.5 Estimation of total starch content using Lugol's iodine

Starch is the main photosynthetic carbon sink. The total starch content produced by the CC-125 cells was estimated using Lugol's iodine (Black et al., 2013). The cells were first bleached by washing with 95% ethanol (as described in section 2.3.4) and then incubated at 100 ℃ along with Lugol's solution for 15 min. The cells were lysed upon boiling and the cellular starch solubilized in Lugol's solution was separated from the cell debris by centrifugation at 10,000 x g for 2 min and discarded. The solubilized starch was estimated in the form of starch-Lugol's complex at 595 nm (OD_{595}) in a multi-mode microplate reader (BioTek Synergy HT, now called Agilent) with path-length correction of 1 cm. The final starch content was obtained in arbitrary units (a.u.) per mL (a.u/mL) and a.u. per 10^6 cells, after normalizing the absorbance with the experimental controls.

2.3.6 Estimation of neutral lipid content using Nile red dye

The neutral lipids synthesized by microalgae under stress are stored in the form of triacylglycerol (TAG) enclosed in lipid droplets (LD). LDs were stained using Nile red dye (Sigma-Aldrich Pt. Ltd). The CC-125 cells were incubated for 10-15 min at 25-28℃ in dark with Nile red dye solution in DMSO at a final concentration of 1 µg/mL (Chen et al., 2009; Kou et al., 2013). Nile red forms a complex with TAG molecule whose fluorescence was captured using a filter set with $\lambda_{ex} = 485 \pm 20$ and $\lambda_{em} = 590 \pm 35$ in a multi-mode microplate reader (BioTek Synergy HT, now called Agilent). The final TAG concentration was calculated in fluorescence units (f.u.) per mL and f.u. per 10^6 cells after normalizing the readings with the experimental controls.

2.3.7 Epifluorescence live-cell imaging of lipid droplets

Lipid droplets were stained with 1 µg/mL Nile red dye, as described in Section 2.3.6. Post-staining, cells were observed with Olympus BX53F2 upright optical microscope in epifluorescence mode, using a 130 W U-HGLGPS excitation source, TRITC filter, and 100X (1.4 NA) Olympus oil-immersion objective. In all the measurements, ~100 cells were imaged with an Olympus DP74 camera. An autotrophic control with no stress exposure was also recorded for reference. Images were processed using Image J

software (Fiji). Briefly, individual cells were selected and analyzed for the total fluorescence intensity of a cell (pixels), size of the lipid droplets (μm^2) contained in a cell, size of the cell (μm^2), and fluorescence intensity of the lipid droplets occupying the cell (pixels), using a custom-made program. The percent area of the cell occupied by lipid droplets (φ) was calculated for LLPS analysis.

2.3.8 Total RNA extraction and quantitative real-time PCR

The RNA extraction was done using the TRI Reagent from Sigma-Aldrich Pt. Ltd. as described by Bell et al. (2016). Here, ~5×10^6 *Chlamydomonas* cells were homogeneously mixed in TRI Reagent and the mixture was subsequently treated with chloroform. The total RNA extracted in the aqueous layer was then precipitated by isopropanol; the precipitated RNA pellet was washed with chilled 70% ethanol and treated with DNase I (final concentration, 1 U) at 37 °C for 40 min. The total RNA was quantified using a Nano-spectrophotometer. A total of ~1 µg of RNA was converted to cDNA using Anchored Oligo dT primers from Verso cDNA synthesis kit, ThermoFisher Scientific Inc. The reaction for qPCR contained ~6 ng of cDNA sample along with TB Green Premix Ex Taq II (Tli RNase H Plus) from Takara Bio Inc., and qRT-PCR was performed on the Applied Biosystems StepOne Real-Time PCR system. Gene-specific primer pairs were designed using Primer 3 software and are given in **Table 2.1**. The primer specificity is shown on gel electrophoresis, see Appendix A2.1. *RACK1* was used as a housekeeping gene and primers for *DGAT* and *RACK1* were used as already reported (Lv et al., 2013). All the experiments were performed in triplicates to check reproducibility and fold change ($\mathbf{2^{-\Delta\Delta C_T}}$) was calculated as given in **Equations 2.7 & 2.8**, where C_T is the cycle threshold of the sample. The representative amplification plots and the melt curves are shown in Appendix A2.2 and A2.3.

$$\mathbf{\Delta\Delta C_T = \Delta C_T\,(Stress\ culture) - \Delta C_T\,(Control\ culture)}$$

Equation 2.7. The equation for calculating $\Delta\Delta C_T$

$$\mathbf{\Delta C_T = C_T\,(gene\ of\ interest) - C_T\,(RACK1)}$$

Equation 2.8. The equation for calculating ΔC_T

Table 2.1. Gene-specific primers designed for quantitative real-time PCR

Gene	Protein product	Protein function	Forward primer (5'-3')	T_m (°C)	Reverse primer (5'-3')	T_m (°C)	T_a (°C)	Amplicon size (bp)
ACC	**A**cetyl-**C**oA **C**arboxylase	Carboxylates the acetate molecule to form acetyl-CoA	CATCATCTCGGTGGTC ATTG	59.1	GCGTTCTCCATGATCA GGTT	59.1	57.3	87
ATG4	**A**u**T**opha**G**y-related protein 4	Activates ATG8 leading to autophagosome formation	ACTGGGCATGGACAA GATCA	59	TCGAGGTAGATGAAG GACGC	58.9	59.4	357
ATG8	**A**u**T**opha**G**y-related protein 8	Autophagosome formation	CGCATCAAGGAGAAG TACCC	58.9	TGCGGATGACGTACA CAAAT	58.9	53	468
PhoA	Starch phosphorylase A	Reversible transfer of glucose-1-phosphate units from heteroglycan chain	TACCTGCGCCTGTACT TCCT	59.1	GATCAGGCAACCGTTC ATCT	59.1	59.4	312
DGAT	**D**iacyl**G**lycerol **A**cyl**T**ransferase	Catalyzes the acylation of DAG to TAG	CCAAGGTGGCTCGTG ACTC	59	ACTCGCCTCTGTGCCT GTT	58.9	61	110
RPS6	**R**ibosome **P**rotein **S6**	Component of 40S ribosomal subunit, involved in translation	TACGTCACCATCTACT CGCG	59.2	GCGTCGGTCTTGTTCT TCTC	59.5	59.4	339
RACK1	**R**eceptor For **A**ctivated **C** **K**inase 1	House-keeping gene	TCAACATCACCAGCA AGAAGG	59.5	CTGGGCATTTACAGGG AGTG	60.5	59.4	131

T_m: Melting temperature, T_a: Annealing temperature

2.3.9 Statistical analysis

The reported values were derived from an average of three independent biological replicates, and the errors represent the standard deviation (S.D.). Statistical significance of the data was obtained by Student's t-test analysis performed in MS Excel, where the data was considered significant only if $p \leq 0.05$. The maximum significance of the data was obtained with $p \leq 0.0001$.

2.4 Results

2.4.1 Determination of cell density from OD_{680}

To avoid cell count in every experiment, cell density was determined from a range of OD_{680} values using a haematocytometer, as described in Section 2.3.3. A linear correlation was obtained between OD_{680} and the cell count (**Figure 2.3**). As the absorbance of the culture sample increased, the cell count increased linearly. This correlation was fit using a linear equation from which the slope of the line and the x-intercept were obtained and put into the equation (y = mx +c) to obtain a universally accepted equation of cell density (**Equation 2.9**). This equation was used at all times to calculate cell count directly from the OD_{680}.

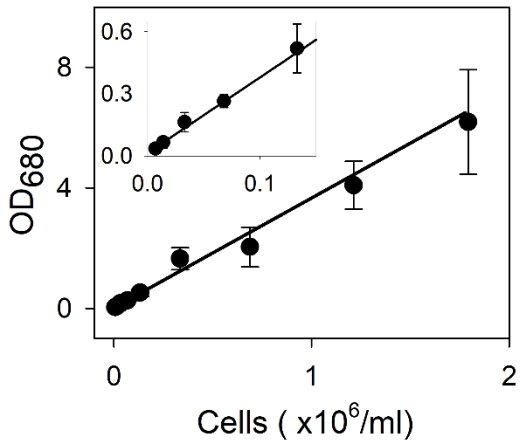

Figure 2.3. Linear plot of cell density measured using haematocytometer at the corresponding OD_{680}.

The scatter points were fit to a linear plot in OriginPro 9.0 software and the linear equation was derived. The inlet in the graph represents closely placed scatter points corresponding to OD_{680} 0.01 to 0.6. The error bars represent the standard deviation from three independent biological replicates.

$$Cells\left(\times\frac{10^6}{mL}\right)=\frac{OD_{680}-0.015}{3.64}$$

Equation 2.9. Linear correlation of OD_{680} and cell density in million cells/mL.

2.4.2 Growth and cell density production in *C. reinhardtii* under salt stress

C. reinhardtii CC-125 grown under optimum conditions in the present laboratory setup has the logarithmic phase of growth lasting for 4 days after which it enters the stationary growth phase. The cultures were monitored for 15 days of growth. We initiated the study with low salt concentration and explored the variations under two-stage cultivation only. As explained in Section 2.3.2, we imposed the microalgal cells with 100 mM NaCl in different ways all grown under photoautotrophic growth: single-stage cultivation in which 100 mM NaCl was applied right at the stage of inoculation (SS_100) and two-stage cultivation where 100 mM NaCl was applied after cultivation in the salt-free medium for 2 days (D2_100) or 4 days (D4_100) (**Figure 2.1**). An autotrophic control with no salt was set for reference. The growth profiles of *C. reinhardtii* cells under the above conditions are shown in **Figure 2.4**. Overall, the addition of 100 mM NaCl showed no significant change in the growth profile. While the cell density gradually starts to decline after the 4th day in the case of Control, the presence of salt in both single-stage and two-stage proves beneficial to the microalgal cells and they do not enter the death phase like the Control. The maximum cell density is obtained in the Control on the 4th day of growth, which is 0.21 ± 0.05 million cells/ml. In presence of 100 mM NaCl, maximum cell density was obtained at the end of 15 days of growth, *viz.* 0.3 ± 0.009 million cells/ml in SS_100, 0.24 ± 0.018 million cells/ml in D2_100, and 0.2 ± 0.016 million cells/ml in D4_100. Among all the culture conditions studied, SS_100 yields the maximum cell density. These results show that the presence of 100 mM NaCl leaves no negative impact on the growth of *C. reinhardtii*.

Figure 2.5 depicts the effect of higher salt concentrations, 150 mM and 200 mM on the growth of *C. reinhardtii*, where we introduced the gradient strategy of cultivation. Two different step sizes were used, salt added at an interval of 1 day (g15_10_150 and g20_10_200) and salt added at an interval of 2 days (g30_10_150 and g40_10_200) (**Figure 2.2**). Cultures incubated with 150 mM NaCl, g30_10_150 (step size of 2 days)

showed the highest cell density accumulation of 0.35 ± 0.06 million cells/ml on the 15th day. On the other hand, g15_10_150 (step size of 1 day) and SS_150 were the most adversely affected conditions. The addition of 200 mM NaCl in SS_200 proves to be the most detrimental for growth. The gradient culture strategies, g20_10_200 and g40_10_200, caused improved cell density accumulation as compared to SS_200 and D4_200, while in D4_200, there was better cell growth than in SS_200, the density was still less when compared to the Control. Thus, the gradient mode of cultivation improved cell growth over the two-stage mode of cultivation which was even better than the single-stage at both the salt concentrations under study *viz*. 150 mM and 200 mM NaCl. Overall, g30_10_150 yields the maximum cell density among all the salt stress conditions.

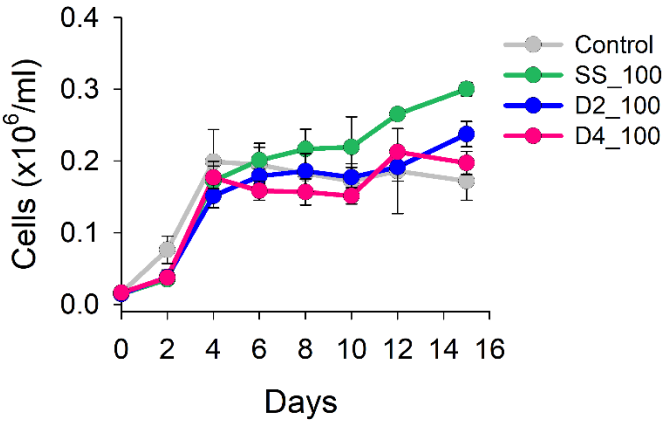

Figure 2.4. Effect of different modes of application of 100 mM NaCl on the growth of *C. reinhardtii* CC-125.

Control represents the autotroph grown in no salt condition, **SS_100** represents the single-stage salt stress where 100 mM NaCl was applied at the beginning of the growth, **D2_100** represents the two-stage culture where 100 mM NaCl was added on the 2nd day of the growth, and **D4_100** is the two-stage where salt was added on the 4th day of growth. The error bars represent the standard deviation derived from the three independent biological replicates.

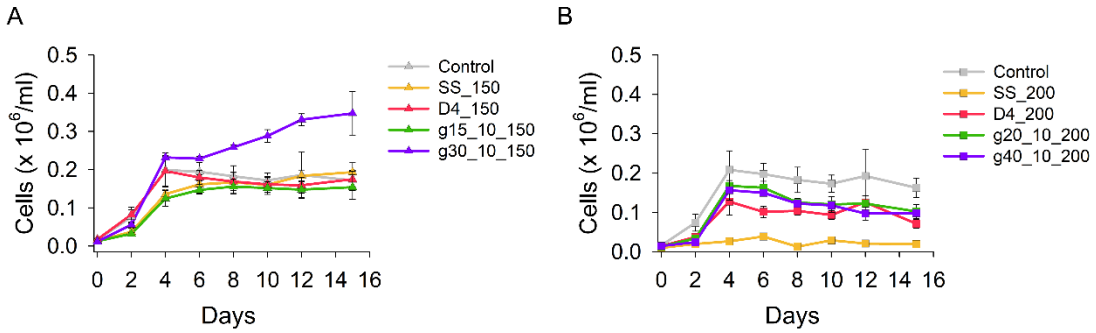

Figure 2.5. Effect of different modes of application of 150 mM and 200 mM NaCl on the growth of *C. reinhardtii* CC-125.

A denotes the cell density in presence of 150 mM NaCl and **B** denotes the cell density in presence of 200 mM NaCl. Here, "**SS**" stands for single-stage, and "**D4**" means two-stage where NaCl was added on the 4th day of growth. **g15_10_150** and **g20_10_200** have 15 mM and 20 mM NaCl, respectively, added daily up to 10 days of growth, while **g30_10_150** and **g40_10_200** have doubled the NaCl concentration, i.e., 30 mM and 40 mM, respectively, added on alternate days up to 10th day of growth. The error bars represent the standard deviation derived from the three independent biological replicates.

2.4.3 Chlorophyll and carotenoid production in *C. reinhardtii* under salt stress

Often under salt stress, microalgae suffer from poor photosynthesis rate (Ji et al., 2018). To analyze this, the effect of NaCl on the production of photosynthetic pigments, i.e., chlorophylls and carotenoids was carried out. The concentration of total chlorophyll (Chl *a* and *b*) and total carotenoids were obtained at four specific time points of the growth cycle, *viz.* day 4 in the log phase, day 6 representing the end-log phase, and days 10 and 15 are the stationary phase time points. The measured values are denoted in mg per million cells and mg/ml of the culture. Interestingly, in presence of 100 mM NaCl, the chlorophyll and carotenoid content increased (**Figure 2.6**). The increase is significantly higher in SS_100 and D2_100 at the stationary phase of growth. Moreover, the content increases as the culture progress from the log phase to the stationary phase. The maximum production of carotenoids and chlorophylls was obtained in SS_100 on day 15, i.e., 6.3 ± 0.64 mg/ml and 30.45 ± 3.6 mg/ml, respectively.

When subjected to the salt stress of 150 mM NaCl (**Figure 2.7**, SS_150), *C. reinhardtii* showed increased accumulation of carotenoids and chlorophylls throughout the growth period. Condition g30_10_150 also resulted in enhanced production of these photosynthetic pigments, especially significant on the 15th day of growth. Since the cell density achieved in the g30_10_150 condition is also the maximum, it delivers the highest yield of carotenoids and chlorophylls, i.e., 6.02 ± 1.1 mg/ml and 28.9 ± 2.8 mg/ml, respectively. In the case of 200 mM NaCl (**Figure 2.8**), there is a significant drop in the total carotenoid and chlorophyll production. Since under SS_200 treatment, the culture did not grow at all, it was not considered for further study. Subsequently, the lowest pigment content was observed in D4_200 most likely attributable to the poor cell density. Similarly, the gradient cultures with 200 mM NaCl also show a significant reduction in pigment accumulation.

Overall, the results signify that the single-stage with 100 mM and 150 mM NaCl show increased production of photosynthetic pigments. The highest carotenoid and chlorophyll yield is obtained in the presence of 100 mM NaCl, with single-stage SS_100. At high NaCl concentrations (150 mM and 200 mM NaCl), stress induces negative effects on the photosynthetic pigment accumulation, however, the gradient strategy helps in improving the net accumulation over two-stage and single-stage.

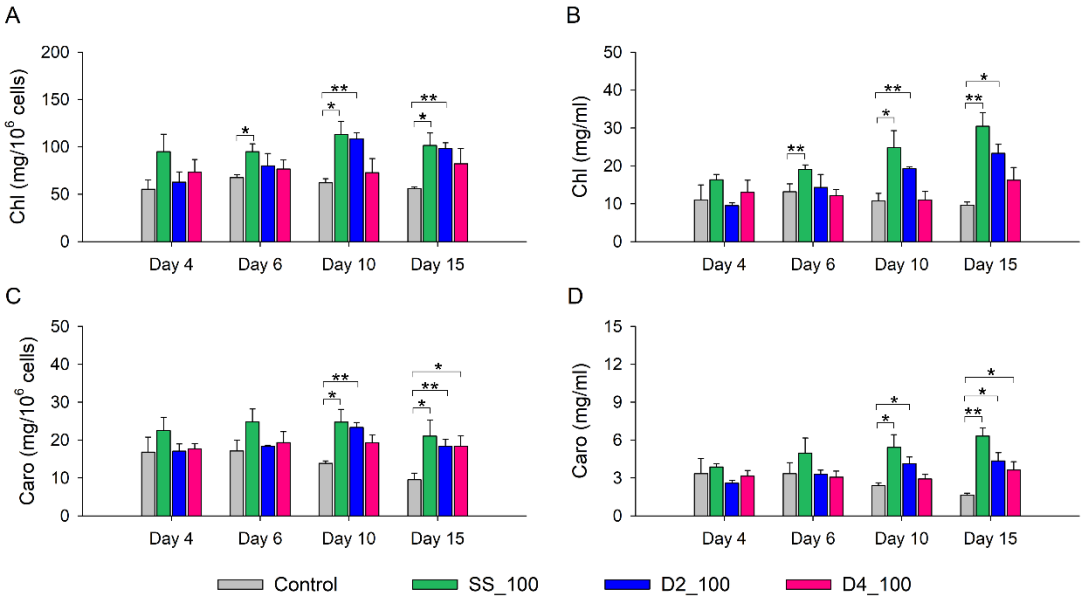

Figure 2.6. Effect of different modes of 100 mM NaCl application on the photosynthetic pigment production in *C. reinhardtii* CC-125.

Here, **A** and **B** represent the total carotenoid content in mg per million cells and mg/ml, respectively. **C** and **D** represent the total chlorophyll content in mg per million cells and mg/ml, respectively. Error bars represent standard deviation for n = 3. *$p \leq 0.5$, **$p \leq 0.01$.

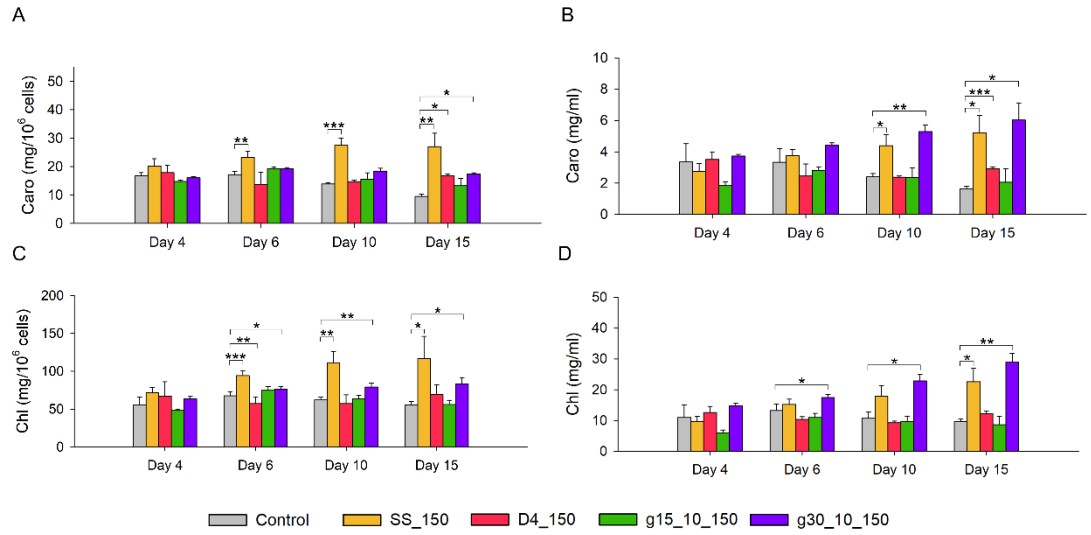

Figure 2.7. Effect of different modes of 150 mM NaCl application on the photosynthetic pigment production in *C. reinhardtii* CC-125.

Here, **A** and **B** represent the total carotenoid content in mg per million cells and mg/ml, respectively. **C** and **D** represent the total chlorophyll content in mg per million cells and mg/ml, respectively. Error bars represent standard deviation for n = 3. *$p \leq 0.5$, **$p \leq 0.01$, ***$p \leq 0.001$

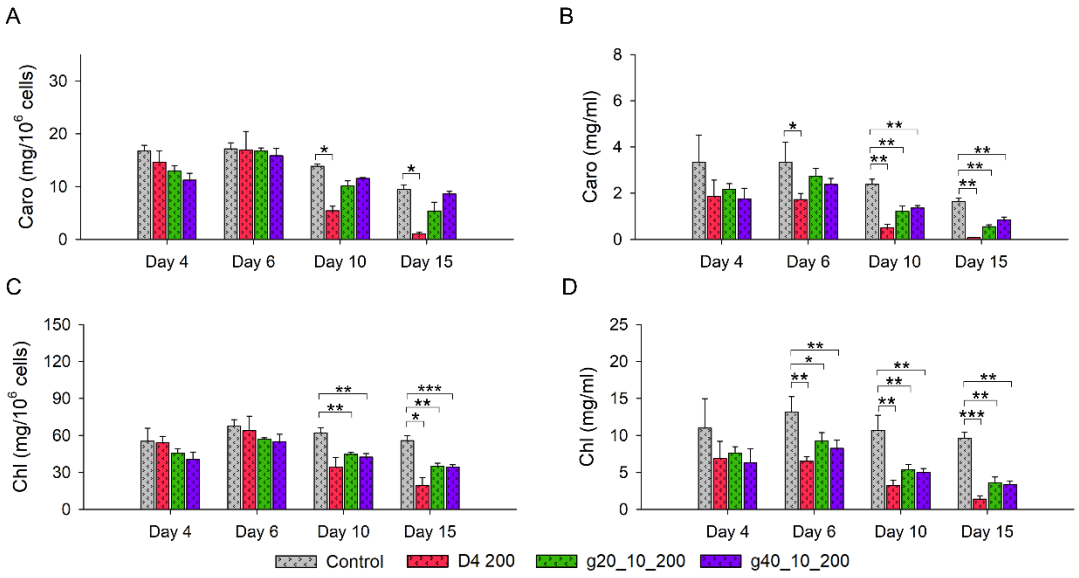

Figure 2.8. Effect of different modes of 200 mM NaCl application on the photosynthetic pigment production in *C. reinhardtii* CC-125.

Here, **A** and **B** represent the total carotenoid content in mg per million cells and mg/ml, respectively. **C** and **D** represent the total chlorophyll content in mg per million cells and mg/ml, respectively. Error bars represent standard deviation for n = 3. *$p \leq 0.5$, **$p \leq 0.01$, ***$p \leq 0.001$

2.4.4 Starch and lipid production in *C. reinhardtii* under salt stress

The present study (Section 2.4.3) shows that 100 mM salt stress increases carotenoid production with no negative effect on photosynthetic pigment accumulation and cell density accumulation in *C. reinhardtii*. To understand the effect of these treatments on starch accumulation, the starch content was measured using Lugol's solution at two specific time points, i.e., days 6 and 10 (**Figure 2.9**) for 100 mM salt stress Interestingly, starch content was found to be significantly higher in all the stress conditions (100 mM concentration) at both time points. A 100-fold higher starch production was obtained from SS_100 on day 10 of cultivation, i.e., 0.46 ± 0.11 units/ml. To study lipid production, the *C. reinhardtii* cells were stained with Nile red after making them permeable with DMSO. Nile red stains neutral lipids effectively, and fluorescently stained lipid droplets in about ~100 cells were imaged with an epifluorescence microscope. The average fluorescence intensity observed in all the cells was calculated (**Figure 2.10)**. Interestingly, the Nile red fluorescence intensity is the highest in D2_100, on both days 6 and 10. This indicates that the neutral lipid/TAG accumulation is maximum in D2_100. Overall, single-stage production with 100 mM NaCl proved beneficial to increase the cell density, pigment, and starch production in *C. reinhardtii*, while two-stage cultivation D2_100 benefits the TAG production.

Examination of 150 mM and 200 mM stress conditions showed that the maximum starch content is obtained on day 4 in both 150 mM and 200 mM NaCl. TAG content reaches the maximum on day 6 in presence of 150 mM and on day 15 in presence of 200 mM NaCl. In the presence of 150 mM NaCl (**Figure 2.11**), there is a marked increase in starch production as well as starch yield in SS_150 throughout the growth cycle. D4_150 also shows an enhanced starch accumulation on day 6. g30_10_150, on the other hand, has improved yields of starch from day 10 onwards because of the high cell density. The maximum starch yield of 0.3 ± 0.04 units/ml was obtained from SS_150 on day 10. On the contrary, TAG production was observed to be compromised in SS_150 and significantly higher in g15_10_150. Despite poor cell density in g15_10_150, it yields the maximum TAG of 36.18 ± 4.6 units/ml on day 6. In the presence of 200 mM NaCl (**Figure 2.12**), starch content in the cells is higher as compared to the Control, especially in the end-log and early stationary phase of growth (days 6 and 10). The net production of starch declines in the Control culture after the log phase, therefore on a comparative scale, the final yield of starch in stressed

conditions is increased. Significantly high starch yields are obtained in the case of gradient cultures (**Figure 2.12**). TAG production was observed to be compromised in presence of 200 mM NaCl. The TAG production was observed to increase only during the late stationary phase of growth, day 15. However, poor cell density yields resulted in a non-significant increase in the TAG yield. The significant changes are quantified by the p-values, as shown in **Figure 2.12** in all cases. Overall, since 200 mM NaCl resulted in compromised growth, it did not prove to be beneficial in the production of bioenergy feedstock.

Hence, the study illustrated that the mode of cultivation is a key factor in diverting the metabolite production pathway from starch to lipid or vice versa. The stress response is dose-dependent, and 100 mM NaCl showed no effects of stress on the microalgal cells, while 200 mM NaCl showed lethal effects. The gradient cultivation strategy helps in building cell density better than the two-stage strategy. The presence of 150 mM NaCl yields the highest cell density and lipid content.

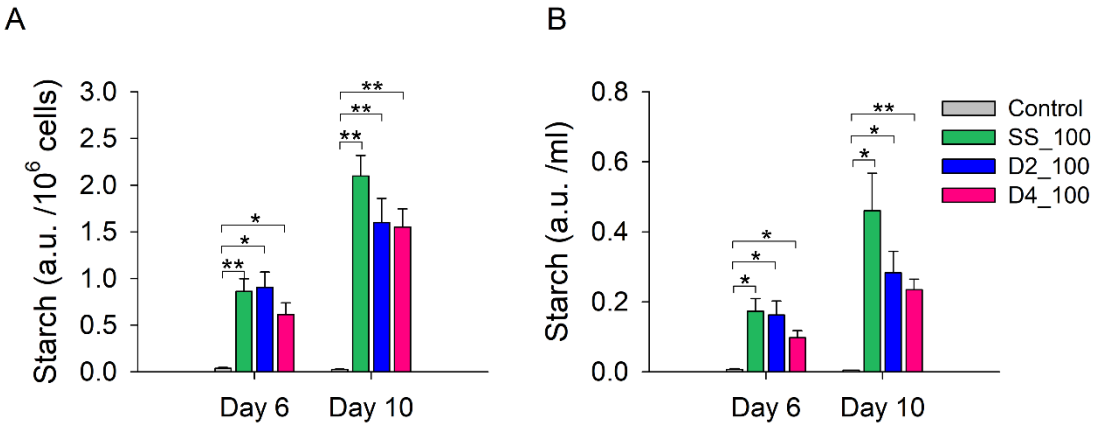

Figure 2.9. Starch production in *C. reinhardtii* in presence of 100 mM NaCl

A denotes the starch production in absorbance units (a.u.) per million cells and **B** denotes the starch content in a.u. per ml of the culture, signifying the starch yield. The observations were made on days 6 and 10 (the end-log phase and the stationary phase). Error bars represent standard deviation for n = 3. $*p \leq 0.5$, $**p \leq 0.01$. Significance increases as the *p*-value decreases

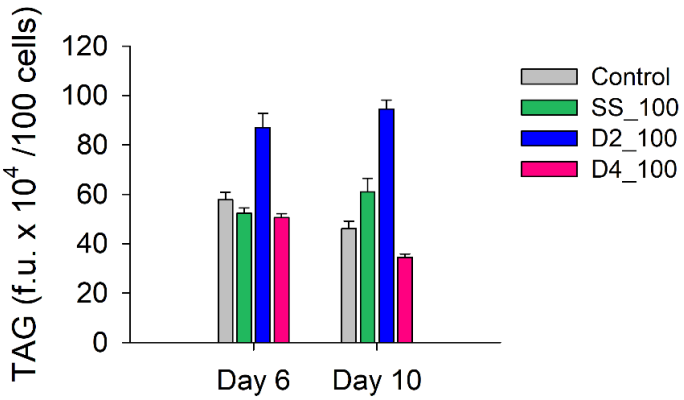

Figure 2.10. TAG production in *C. reinhardtii* under 100 mM NaCl as detected by Nile red fluorescence microscopy.

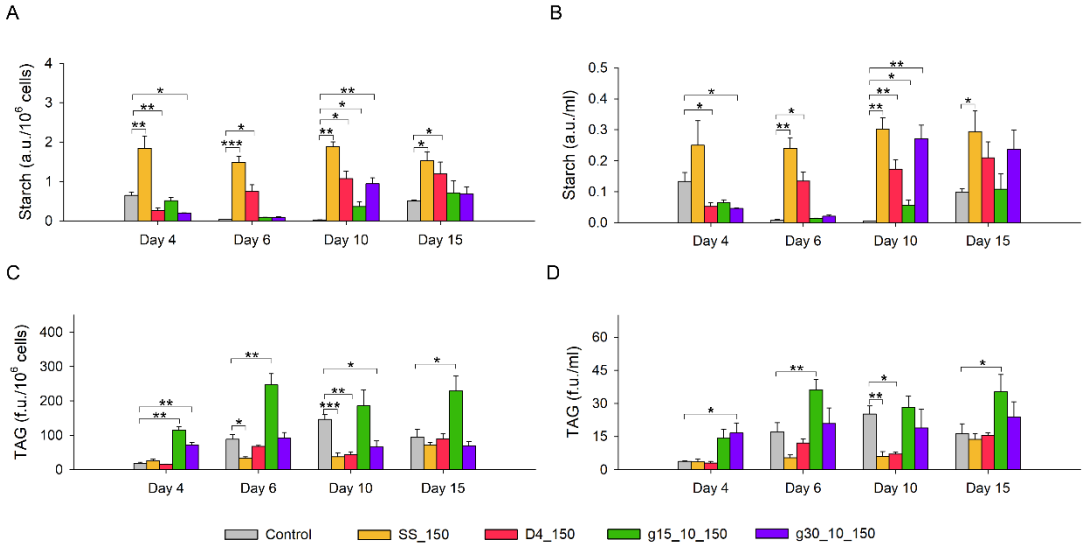

Figure 2.11. Starch and TAG production in *C. reinhardtii* in presence of 150 mM NaCl.

Here, **A** and **B** represent the starch content in a.u. per million cells and ml, respectively. **C** and **D** represent the TAG content in f.u. per million cells and ml, respectively. Error bars represent standard deviation for n = 3. *$p \leq 0.5$, **$p \leq 0.01$, ***$p \leq 0.001$

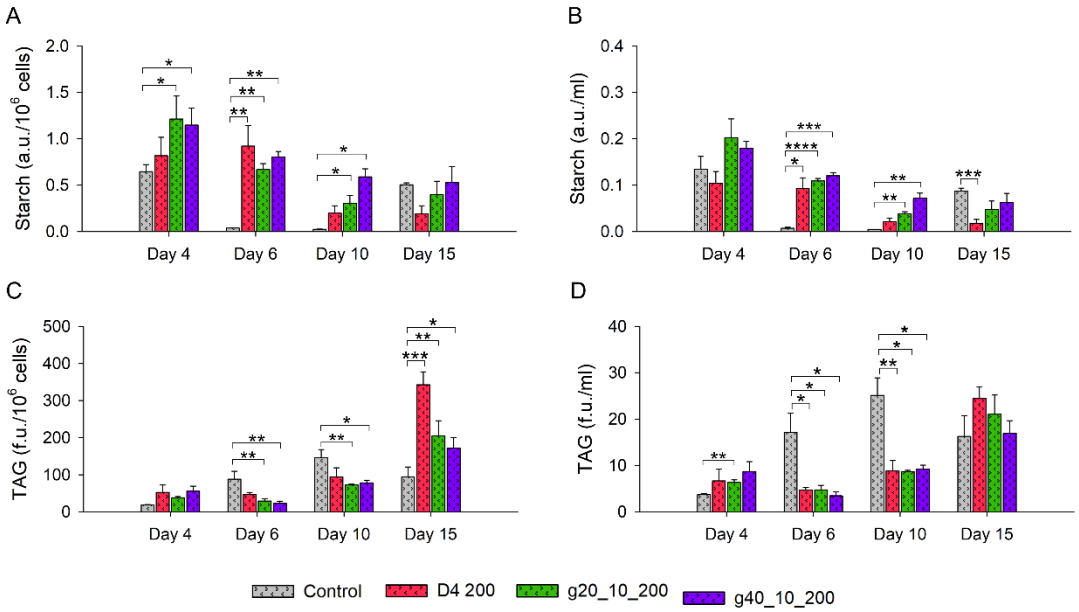

Figure 2.12. Starch and TAG production in *C. reinhardtii* in presence of 200 mM NaCl.

Here, **A** and **B** represent the starch content in a.u. per million cells and ml, respectively. **C** and **D** represent the TAG content in f.u. per million cells and ml, respectively. Error bars represent standard deviation for n = 3. *$p \leq 0.5$, **$p \leq 0.01$, ***$p \leq 0.001$, ****$p \leq 0.0001$

2.4.5 Expression analysis of genes involved in growth, autophagy, and *de novo* lipid synthesis in *C. reinhardtii*

As observed previously, cell density and lipid yields were maximum in the presence of 150 mM NaCl along with a good yield of starch and pigments. Therefore, it was of interest to analyze the expression levels of genes known to play a role in enhanced lipid accumulation under stress. A total of 6 genes were studied, involved particularly in starch degradation (*PhoA*), *de novo* lipid synthesis (*ACC* and *DGAT*), autophagy (*ATG4* and *ATG8*), and protein synthesis and autophagic flux (*RPS6*). The expression level of these genes in single-stage, two-stage, and gradient cultivations was studied in comparison to the housekeeping gene, *RACK1* on the 4th day (log phase) and 10th day (stationary phase) of the growth (**Figure 2.13**). *ATG4* and *ATG8* are the autophagic genes responsible for coding AuTophaGy-related proteins, ATG4 and ATG8. Together, they assist in autophagosome formation induced by stress and result in the catabolic breakdown of membrane lipids, thereby increasing the carbon pool (Pérez-Pérez et al., 2017). *RPS6* codes for ribosomal protein S6, a component of the smaller ribosomal subunit, which plays a vital role in cell growth and is an indicator of autophagic flux (Pérez-Pérez et al., 2017). In this study, both *ATG4* and *ATG8* are highly upregulated in D4_150 and g15_10_150 on day 10. While *ATG4* in g15_10_150 is upregulated by 47.6-folds, *ATG8* is upregulated by 28.9-folds. D4_150 exhibits a 19.7-fold change in *ATG4* levels and a 161.8-fold change in *ATG8*. *RPS6* is upregulated in g30_10_150 on day 4 and D4_150 on day 10. However, D4_150 shows an upregulated expression of both *RPS6* and autophagy-related genes *ATG4* and *ATG8* on day 10. This suggests that two-stage cultivation induces autophagy without involving ribosomal protein turnover. Further studies might shed more light on the same. Besides D4_150, g15_10_150 shows a downregulated expression of *RPS6* and upregulation of both *ATG4* and *ATG8* on day 10, prominently pointing at the active autophagy in action.

Under condition g15_10_150 the culture further shows highly upregulated levels of expression of *ACC*, *DGAT*, and *PhoA* on day 10. *DGAT* codes for the diacylglycerol acyltransferase (DGAT) enzyme which catalyzes the acylation of the DAG molecule to form TAG, and represents the de-novo TAG synthesis pathway (Li-Beisson et al., 2015). *ACC* encodes acetyl-CoA carboxylase, the rate-limiting enzyme which adds the carboxyl moiety to the acetate molecule (Johnson and Alric, 2013). After this step, the carboxy-acetylated molecule is fluxed into the de-novo fatty acid synthesis pathway.

PhoA encodes for starch phosphorylase A which leads to the degradation and formation of glucose-1-phosphate (the first step in lipid synthesis). Starch-to-lipid switching is a well-known phenomenon that aids in the lipid accumulation process under stress (Ho et al., 2017). The current findings suggest a concerted action of *de novo* lipid synthesis, starch degradation, and autophagy regulating the enhanced lipid production (**Figure 2.11**). Further, the increased levels of *ACC* by 125-folds in SS_150 on day 4 signifies the involvement of *de novo* lipid synthesis in lipid accumulation in the single-stage cultivation.

Overall, single-stage cultivation features enhanced levels of *de novo* lipid production in the log phase of their growth. Two-stage cultivation induces autophagy without affecting protein turnover activity. Lastly, the gradient cultivation strategy exhibits highly upregulated levels of autophagy, starch degradation, and *de novo* lipid production.

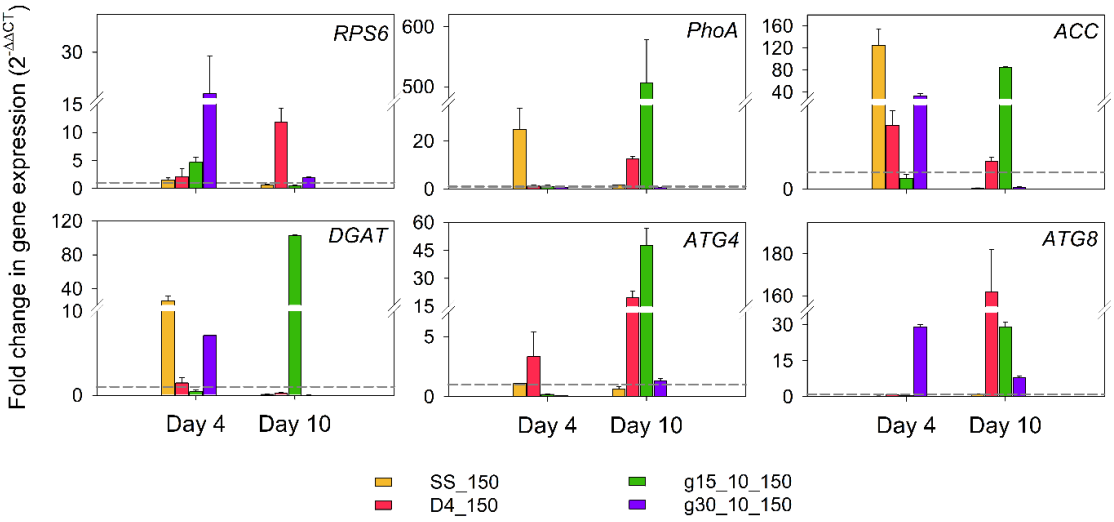

Figure 2.13. Fold change in expression of genes affecting the growth, autophagy, and *de novo* lipid synthesis in *C. reinhardtii* under salt stress.

Fold change ($2^{-\Delta\Delta C_T}$) in gene expression was calculated keeping the autotrophy control as the reference, represented by a gray-colored dashed line at fold change = 1. *RACK1* is the internal control. *DGAT*- Diacylglycerol acyltransferase, *ACC*- Acetyl-CoA carboxylase, *PhoA*- Starch phosphorylase A, *ATG4*- autophagy-related protein ATG4, *ATG8*- autophagy-related protein ATG8, *RPS6*- ribosomal protein subunit. Day 4 represents the log phase and Day 10 represents the stationary phase of the culture.

2.4.6 Cell morphological changes in *C. reinhardtii* under salt stress

2.4.6.1 Under 100 mM NaCl stress

Salt stress is known to induce behavioral as well as morphological changes in microalgal cells (Khona et al., 2016). Hence, a sub-population of salt stress-exposed *C. reinhardtii* cells were imaged by single-cell epifluorescence microscopy to study the typical morphological characteristics like cell size, cell shape, and size of the lipid droplets produced under salt stress. ~100 cells grown in presence of high salt concentrations, *viz.* 100 mM and 150 mM NaCl (as described in section 2.3.2) were observed using a 100X objective (200 mM NaCl was not studied due to poor growth). Most cells were found to exist in the stress-induced palmelloid structure in presence of 100 mM NaCl (**Figure 2.14**). The palmelloid consists of a cluster of cells, protected by a gel-like extracellular matrix, covered by the cell wall. This is a survival strategy adopted by the *C. reinhardtii* cells in extreme environments. The palmelloids have cells with reduced cell size and show a loss of flagella (Shetty et al., 2019). Interestingly, the palmelloid structure develops in D2_100 only on day 10, while the SS_100 stress condition shows prominent palmelloids at all stages of the growth phase. D4_100 stress condition has hardly any palmelloid development. The cell size and shape of the cells in salt stress in ~100 cells were measured from the microscopy images and histograms showing the probability distribution of these properties in the population (**Figures 2.15 & 2.16**) were made. A small subset of the main population was observed to have large-sized cells in D2_100 on day 6, with a hint of the presence of a sub-population on days 4 and 10 with variable parameters compared to the majority of cells. This suggests that two-stage salt stress exerts a differentiation pressure on the cells to bifurcate from the main population and adapt to the changing environment. On the other hand, the cells were observed to shrink in size in SS_100 and D4_100, due to osmotic shock. Overall, the shape of the cells was observed to be largely circular, even under salt stress. However, there exists a prominent sub-population of cells with distorted circularity in SS_100. The distribution in D4_100 is broad and unimodal with the distribution mean lying close to 1 (highly circular). This study suggests that SS_100 is more severely affected by salt stress exposure, while D2_100 represents properties similar to the Control. The size of lipid droplets produced by the microalgal cells in presence of 100 mM NaCl was also measured using the Fiji software (**Figure 2.17**). Lipid droplets were

stained by Nile red and their fluorescence was observed under the epifluorescence microscope. The lipid droplets were found to be distributed in the cytosolic area, prominent in two-stage conditions (**Figure 2.14**). The size of these droplets was found to be the largest in the D2_100 condition on all days of observation (**Figure 2.17**). SS_100 produced large sized-droplets on day 10, however smaller than D2_100. These droplets produced in SS_100 were still larger as compared to the Control. The strong affinity of the lipid molecules towards each other results in large-sized droplets.

Thus, single-stage salt stress results in palmelloid formation and shrinkage of cells possibly due to osmotic stress caused by salt. Two-stage cultivation methods studied here induce different impacts on cellular morphology and lipid droplet development. D2_100 culture shows signs of gradual adaptation to the changing stress condition with very little impact on cell size. It also produces large-sized lipid droplets, as opposed to the other conditions. The possible phenomenon behind the variable size of lipid droplets and the related consequence on cell morphology is explored in detail in the subsequent section.

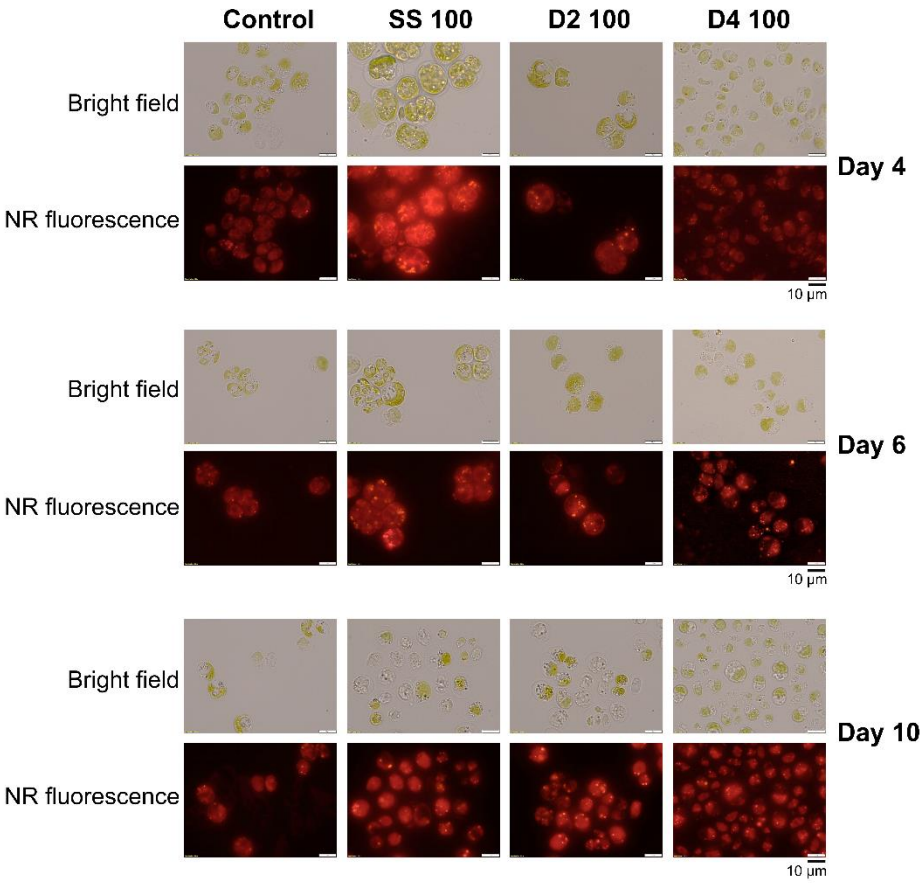

Figure 2.14. Bright-field and Nile red stained epifluorescence microscopic images of *C. reinhardtii* observed at 100 X, grown in presence of 100 mM NaCl.

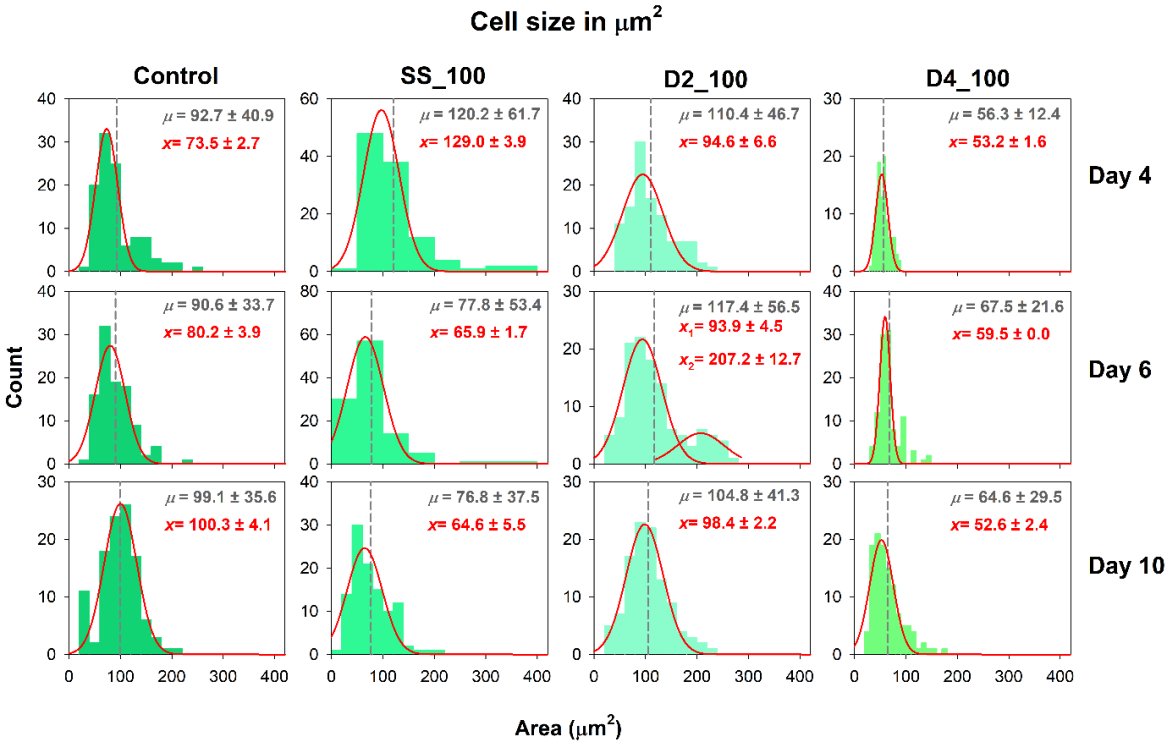

Figure 2.15. Probability distribution of the size of *C. reinhardtii* cells when grown in presence of 100 mM NaCl.

Green-shaded bars represent the histogram of the size of ~100 cells in terms of the area (μm^2), the grey-colored dashed vertical line in each graph represents the population means μ, red-colored graphs represent the normal distribution fit of the histograms and x is the mean obtained from the fit.

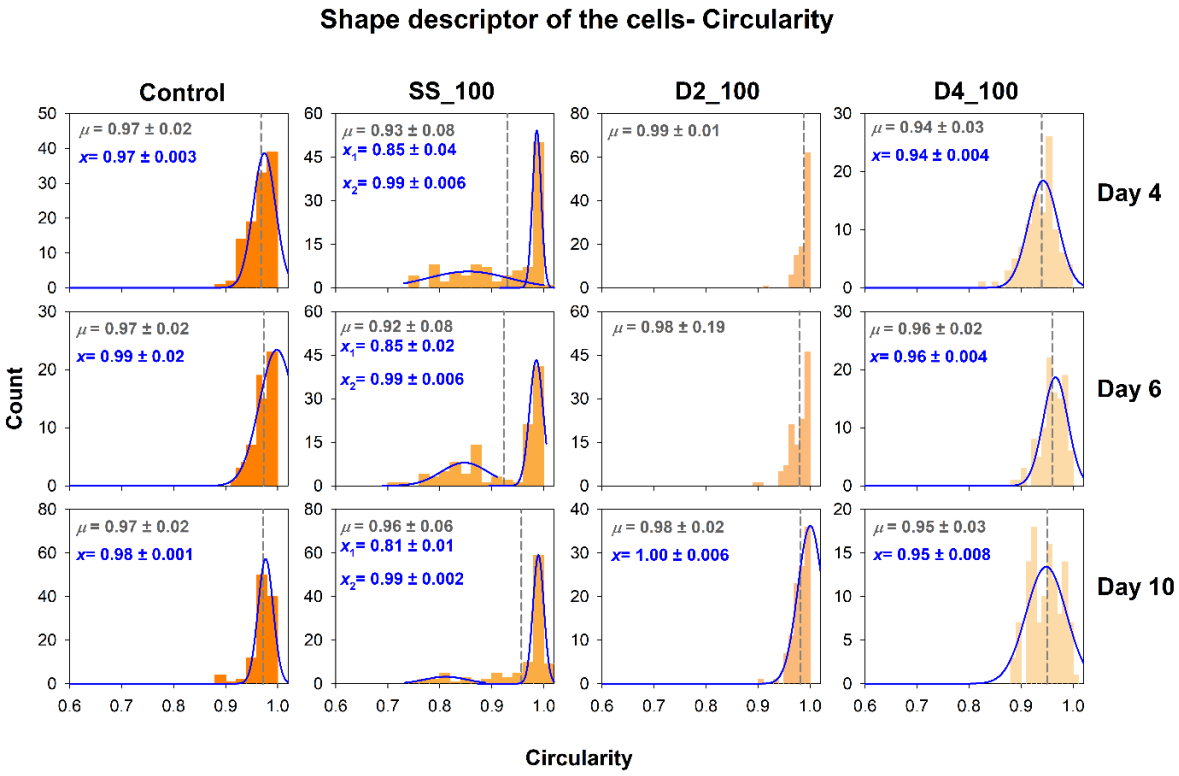

Figure 2.16. Probability distribution of the shape of *C. reinhardtii* cells when grown in presence of 100 mM NaCl.

Orange-shaded bars represent the histogram of the shape of ~100 cells in terms of the circularity, grey-colored dashed vertical lines in each graph represents the population means μ, blue-colored graphs represent the normal distribution fit of the histograms and x is the mean obtained from the fit.

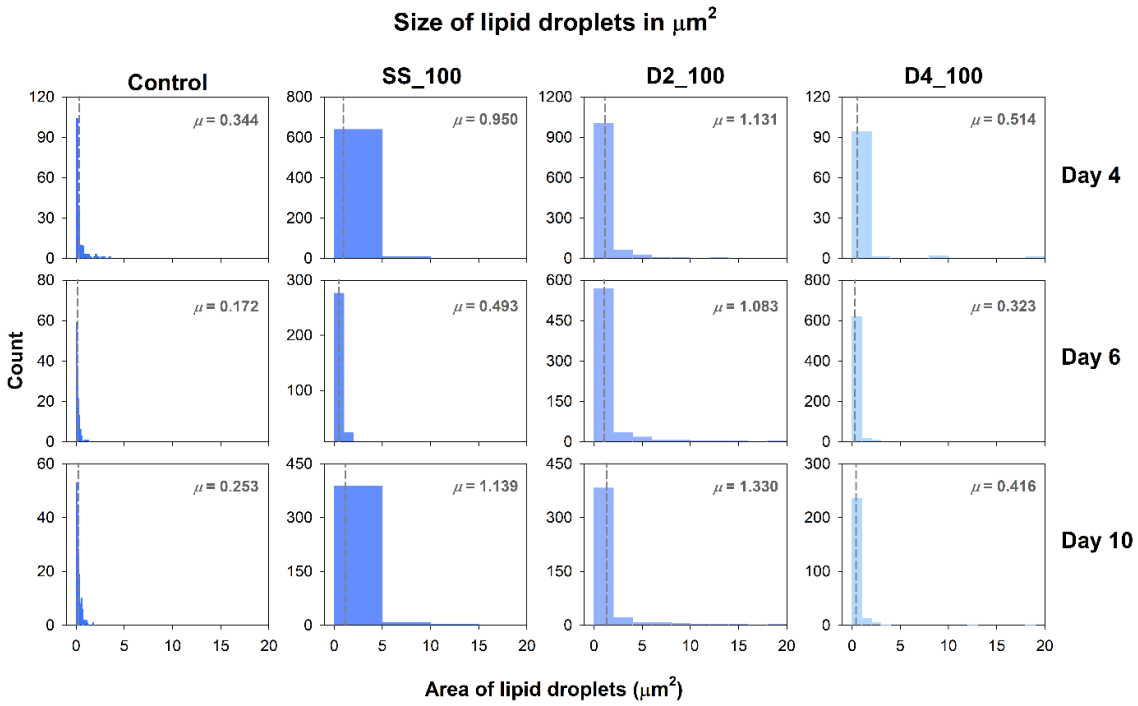

Figure 2.17. Probability distribution of the size of lipid droplets produced by *C. reinhardtii* in presence of 100 mM NaCl.

Blue-shaded bars represent the histogram of the size of lipid droplets produced by ~100 cells in terms of the area (μm^2), and grey-colored dashed vertical lines in each graph represent the population means μ. Since the histograms are not normally distributed, they could not be fitted.

2.4.6.2 Under 150 mM NaCl stress

On identifying the distinct morphological characteristics in presence of 100 mM NaCl, it was motivating to note the changes in presence of higher salt concentration. Thus, these properties were further studied when 150 mM NaCl is present in the external environment. The two very prominent and key features, i.e., palmelloid formation and loss of photosynthetic pigments, were noticed as a function of changing modes of cultivation (**Figure 2.18**). Firstly, a thick layer of palmelloid sheet was observed in SS_150 condition, otherwise very thin in two-stage and gradient cultivations. This was accompanied by the high-order organizations of cells in single-stage, since day 6. The strength of the organization went up to as high as 8 cells on day 10 in SS_150, while it was only 4 cells in two-stage and gradient. Secondly, the pigment content was majorly impaired in D4_150 day 6 onwards. This loss of pigments can also be observed in SS_150 and g30_10_150 on day 10. Since the lipid droplets were found to be majorly distributed in the cytosolic area of the cell, this distribution spreads to the entire cellular area in bleached cells. The cell size distribution (**Figure 2.19**) suggests that the cell size decreases in SS_150, D4_150, and g15_10_150 from day 4 to day 10, while it increases in Control and g30_10_150. The cell size, as compared to the Control, is drastically reduced in single-stage and gradient cultivations on day 6 and under all salt stress conditions on day 10. Thus, step-wise increment of salt concentration does not help in preventing the osmotic shock in *C. reinhardtii* cells and hence the cell size is greatly reduced. However, the cell size in the g30_10_150 condition is suggestively greater than SS_150 on days 6 and 10. This suggests that the step size of salt addition is a more important factor in governing the osmotic pressure on the cell. We also studied the distribution of the cell circularity in the population of microalgal cells under salt stress (**Figure 2.20**). There was no significant difference in the cell shape across the population of stress-exposed cells as compared to the Control, except for the appearance of bimodal distribution in SS_150 on day 4, with a small sub-population having distorted circularity. Sudden exposure to high salt concentration led to the immediate disturbance in cell membrane integrity which got optimized later with time.

Further, the distributions of the average size of lipid droplets produced by the microalgal cells in presence of 150 mM NaCl (**Figure 2.21**) revealed interesting features of lipid droplets as a function of mode of salt stress. Huge droplets were observed in SS_150 on day 4. However, their size began to decrease with age. In

contrast, the droplet size in g15_10_150 was observed to increase with time. Overall, both SS_150 and g15_10_150 cultivations led to the formation of large lipid droplets but at different timelines. The droplet size in g30_10_150 peaked on day 6. D4_150 caused a significant size reduction in their lipid droplet formation. These results suggest that the mode of cultivation plays an important role in governing the size of lipid droplet formation. The smallest change in the step size of salt addition also triggers significant changes in droplet synthesis. It would be interesting to study the physical factors associated with the droplet distribution inside the cell as the function of the mode of cultivation in *C. reinhardtii* under salt stress.

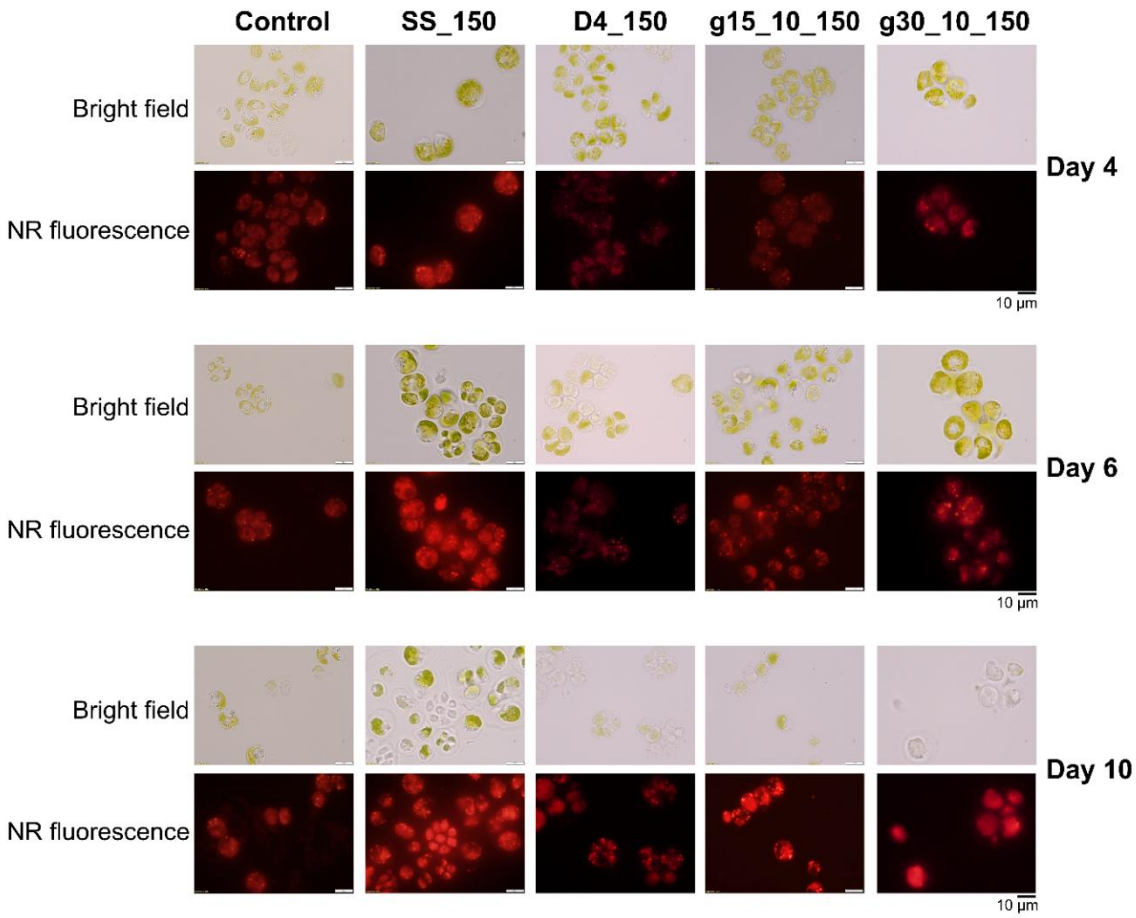

Figure 2.18. Bright-field and Nile red epifluorescence microscopic images of *C. reinhardtii* observed at 100 X, grown in presence of 150 mM NaCl.

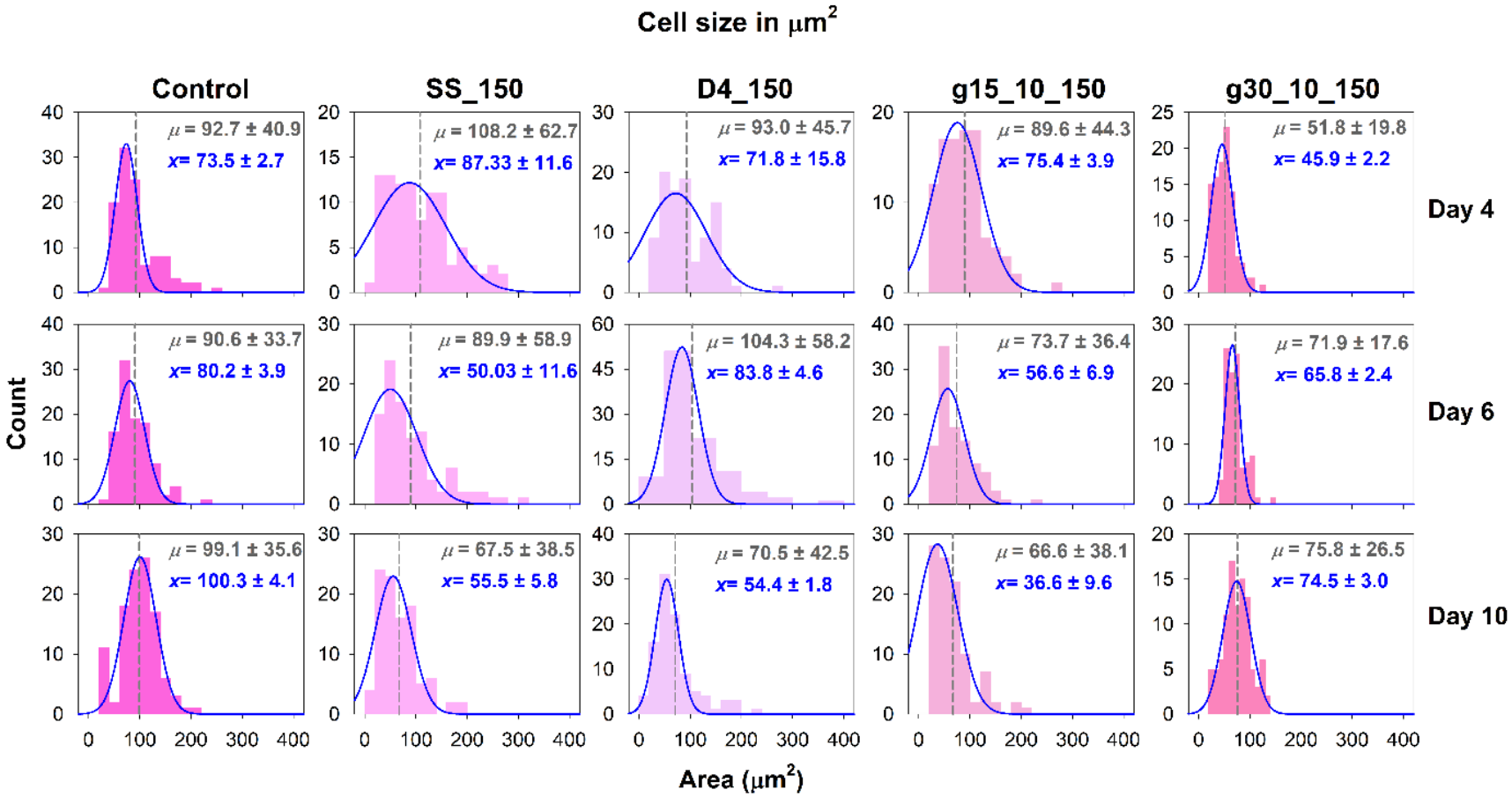

Figure 2.19. Probability distribution of the size of *C. reinhardtii* cells when grown in presence of 150 mM NaCl.

Pink-shaded bars represent the histogram of the size of ~100 cells in terms of the area (μm^2), the grey-colored dashed vertical lines in each graph represent the population means μ, blue-colored graphs represent the normal distribution fit of the histograms and x is the mean obtained from the fit.

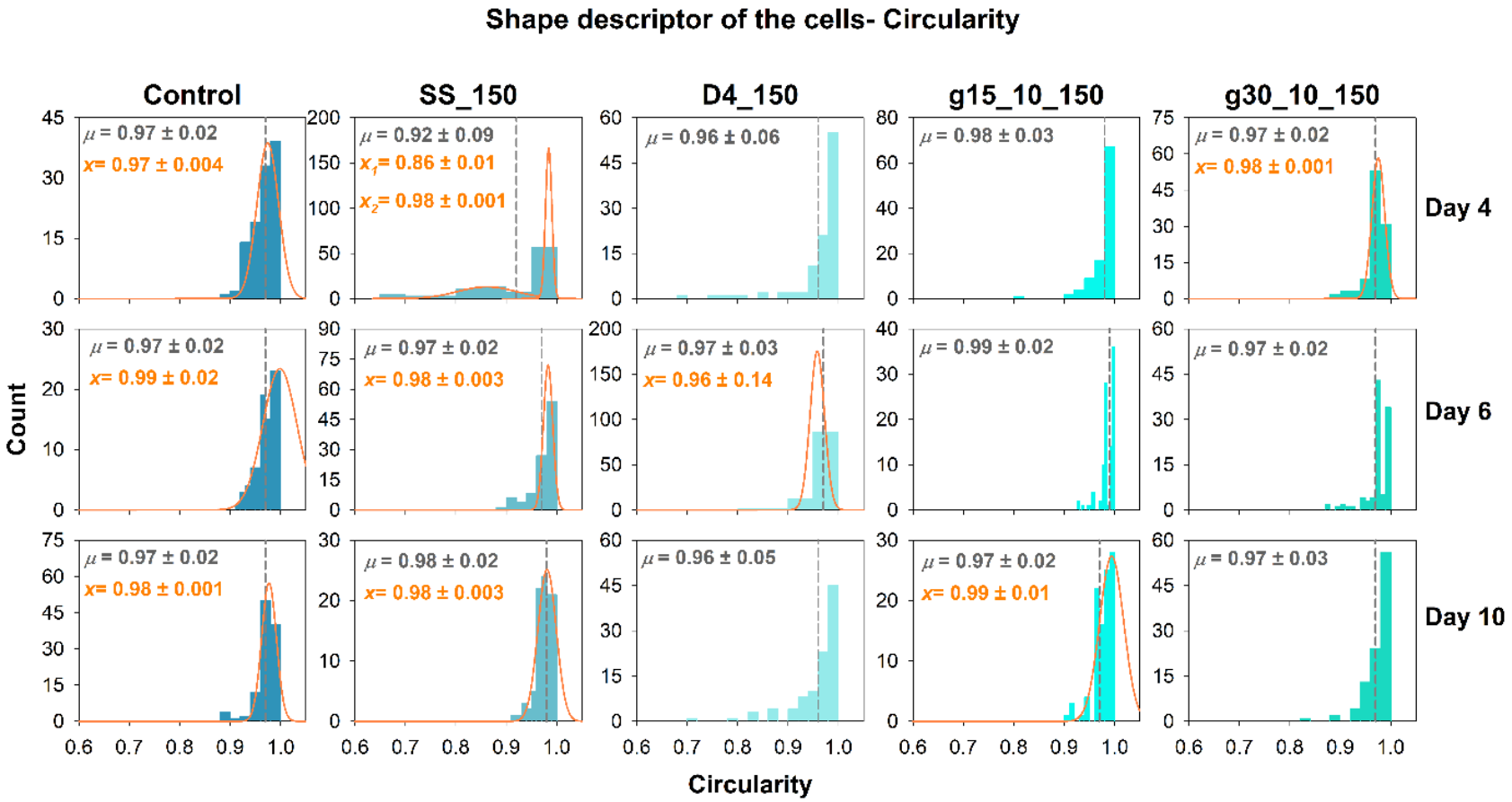

Figure 2.20. Probability distribution of the shape of *C. reinhardtii* cells when grown in presence of 150 mM NaCl.

Cyan-shaded bars represent the histogram of the shape of ~100 cells in terms of circularity, grey-colored dashed vertical lines in each graph represent the population means μ, orange-colored graphs represent the normal distribution fit of the histograms and x is the mean obtained from the fit.

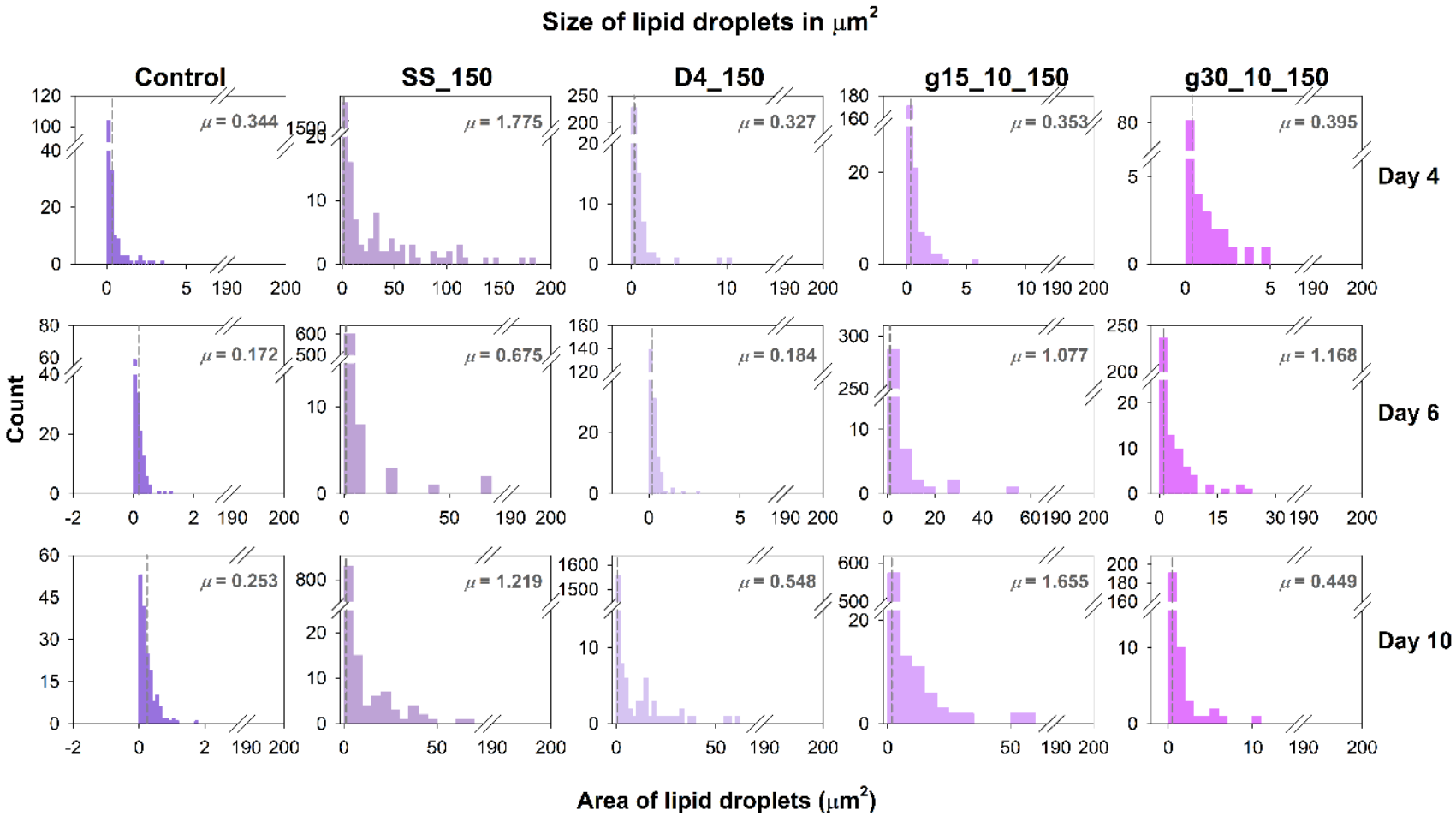

Figure 2.21. Probability distribution of the size of lipid droplets produced by *C. reinhardtii* in presence of 150 mM NaCl.

Purple-shaded bars represent the histogram of the size of lipid droplets produced by ~100 cells in terms of the area (μm^2), and grey-colored dashed vertical lines in each graph represent the population means μ. Since the histograms are not normally distributed, they could not be fitted.

2.4.6.3 Lipid droplet growth dynamics and phase behavior in *C. reinhardtii* in the presence of 150 mM NaCl

The coexistence of the hydrophobic lipid droplets in the hydrophilic cytosol is very interesting since the microscope images reveal reasonably stable droplet structures. Lipid droplet statistics such as the droplet count per area of the cell (**Figure 2.23**) and the percentage area of the cell occupied by these droplets, φ (**Figure 2.24**) were calculated for about 100 cells for each condition, and probability distributions were obtained, which gave the variation (standard deviation) as well as the average parameter analyzed. While the droplet count per area symbolizes the droplet density, the percent area occupied gives an idea of the coexistence ratio of droplets in 2D with respect to the cytosol inside the cell. Fluctuations in the droplet size are quantified by the parameter, α ($\alpha = v/x^2$ where v is the variance in the data, and x is the mean of the variable) (**Figure 2.25**), across a population of ~100 cells for a particular culture condition. The maximum variability is observed in the salt stress conditions when compared to the Control culture. The fluctuations confirm that the heterogeneous distribution in the data is not an experimental artefact and occur due to variable sub-populations in the culture, showing heterogeneous cellular response in cells even within a single population. Further, an increased number of lipid droplets per area of the cell was observed in both SS_150 and g15_10_150, more prominently higher in the single-stage (**Figure 2.23**). Interestingly, it was the highest in D4_150 on day 10. Thus, D4_150 resulted in the production of small-sized droplets (**Figure 2.21**), however more densely packed inside the cell. In contrast, g30_10_150 produced loosely packed but large-sized droplets (**Figure 2.21**). Further, the area occupied by these droplets was also found to be highest in SS_150 on all days of growth, while g15_10_150 showed an increase in the area occupied by their droplets on days 6 and 10 only (**Figure 2.24**). A considerably large area was occupied by droplets in D4_150 on day 10 and g30_10_150 on day 6, suggesting a widespread distribution of droplets. Overall, the droplet distribution varies among different cultivation modes under salt stress.

The total number of droplets was segregated into three categories of different size ranges (as mentioned in the figure caption, **Figure 2.26**). The spatial segregation of the lipid droplets in the cell based on their size showed a rich, salt-stress condition-dependent phase behavior. The maximum number of lipid droplets is observed in SS_150 on day 4 followed by D4_150 on day 10. After proportionating it was found

that this increase is majorly contributed by the small-sized droplets (**Figure 2.26B**). Gradient cultivations result in a low count but a significantly higher proportion of larger lipid droplets (**Figure 2.26A**). These results imply that single-stage and two-stage impose an increase in the smaller lipid droplets while gradient cultivation synthesizes larger lipid droplets. The lipid droplets are usually found to be in the two-phase, or phase-separated state in the cytosol, and different conditions yield different phase coexistence boundaries, as shown in **Figure 2.22** where the 2D area fraction of droplets is plotted as a function of culture age. The shaded regions in this figure denote the two-phase state. The enhanced production of lipids, and increase in droplet size, as well as density, leads to droplets that completely encompass the cytosol, resembling a mixed, one-phase state. This one-phase state mostly commences towards the later part of the stationary growth phase or at the beginning of single-stage salt stress, absent otherwise in the Control culture. Thus, SS_150 possesses the highest amount of two-phased lipid droplets at all phases of growth. Gradient, g15_10_150, shows an increasing population of two-phase droplets along with the culture age. This can be explained by the increasing lipid concentration at the stationary phase (**Figure 2.11**) accompanied by the increased autophagic and anabolic lipid production activities (**Figure 2.13**). These results signify that phase separation plays a crucial role in governing lipid droplet growth dynamics which vary greatly as a function of the culture age and the mode of cultivation. This feature of lipid droplet distribution as measured by the single-cell 2D epifluorescence microscopy would have otherwise remained unseen in the average bulk measurements.

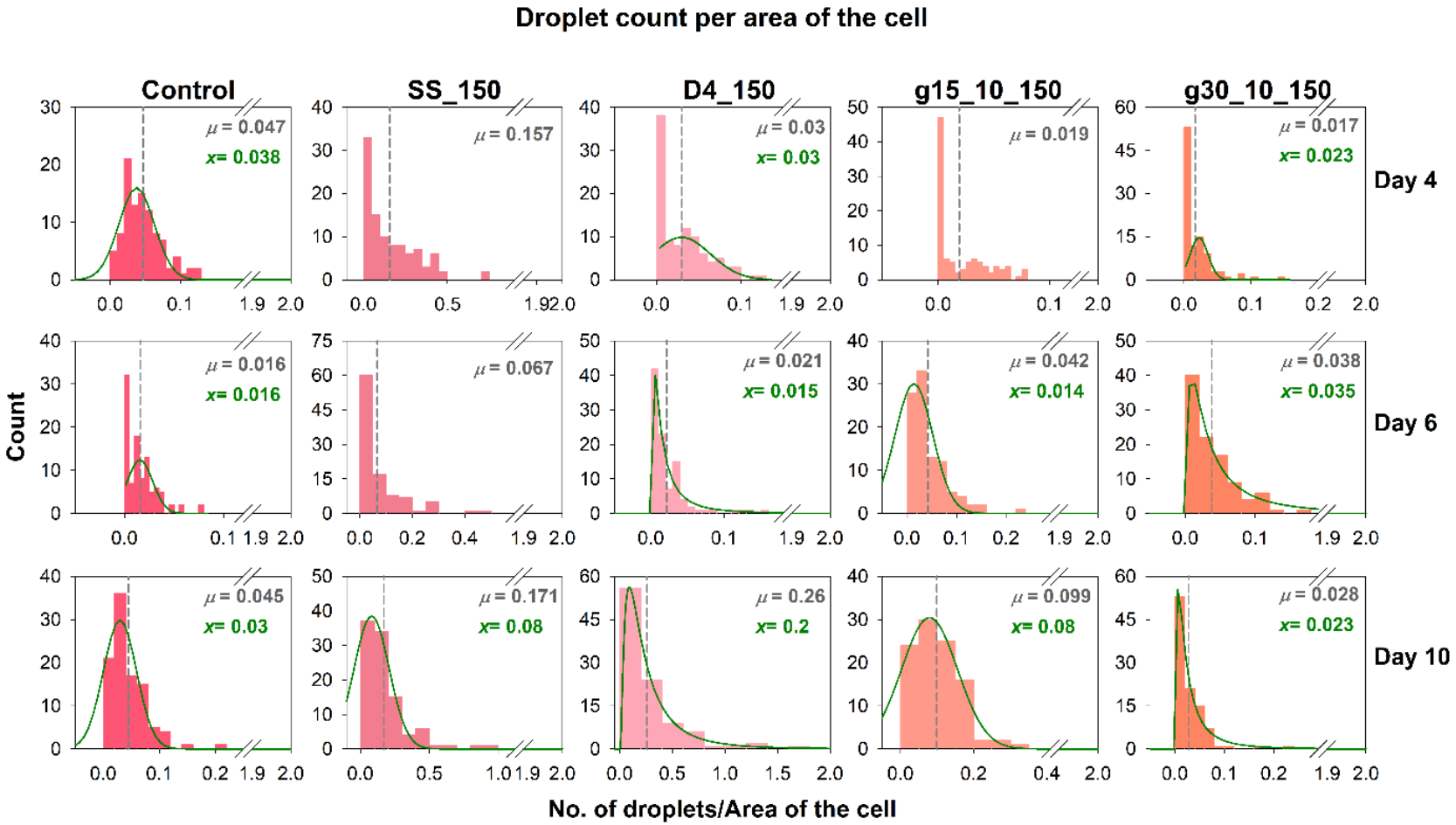

Figure 2.23. Probability distribution of the number of lipid droplets distributed per area of the *C. reinhardtii* cell in presence of 150 mM NaCl.

Red-shaded bars represent the histogram of the size of lipid droplets produced by ~100 cells in terms of the area (μm^2), and grey-colored dashed vertical lines in each graph represent the population means μ. The green-colored graphs represent the normal or log-normal distribution fits with mean *x*.

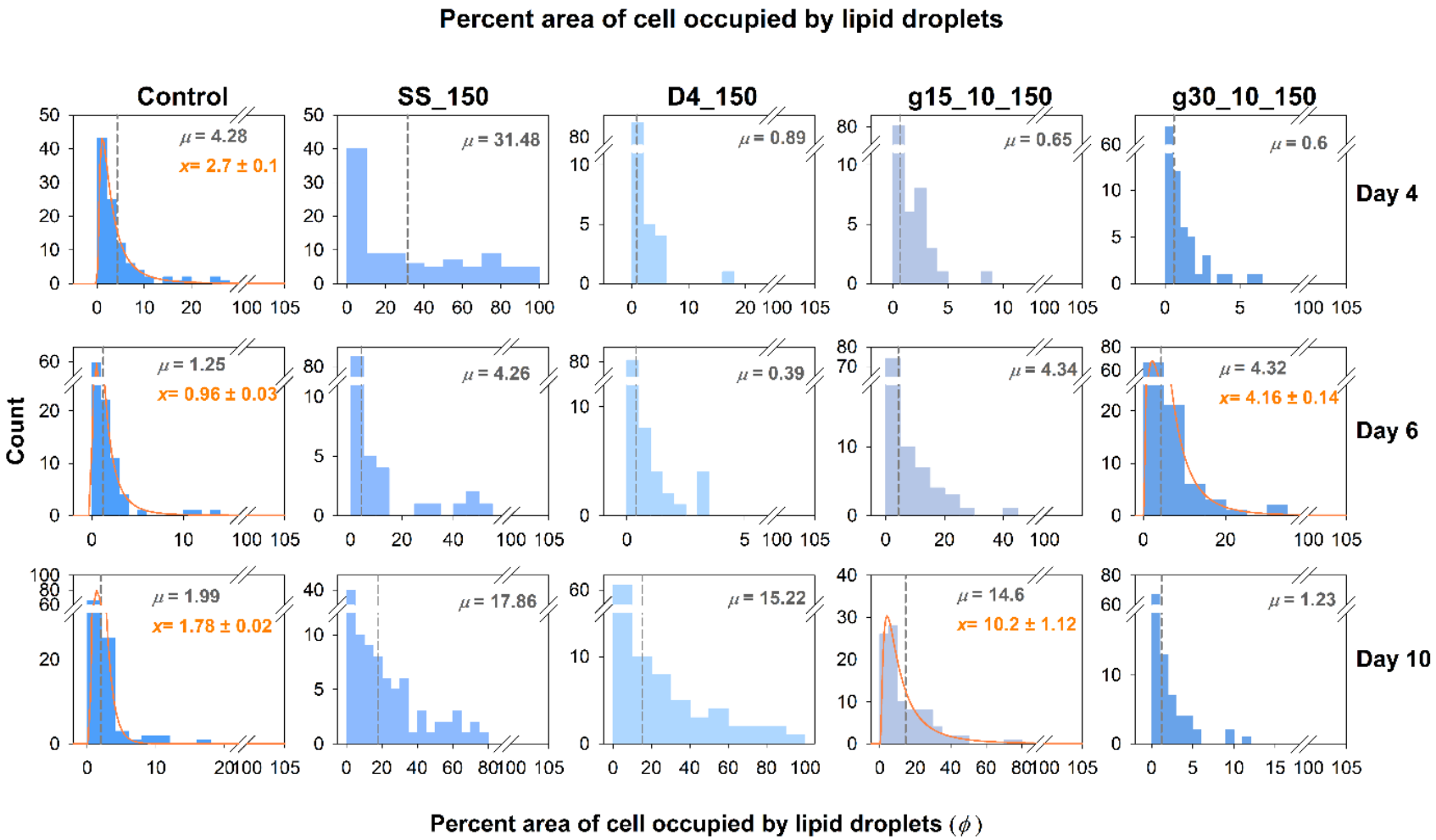

Figure 2.24. Probability distribution of the percentage area of the cell occupied by the lipid droplets produced by *C. reinhardtii* in presence of 150 mM NaCl.

Blue-shaded bars represent the histogram of the size of lipid droplets produced by ~100 cells in terms of the area (μm^2), and grey-colored dashed vertical lines in each graph represent the population means μ. The orange-colored graphs represent the log-normal distribution fits with mean *x*.

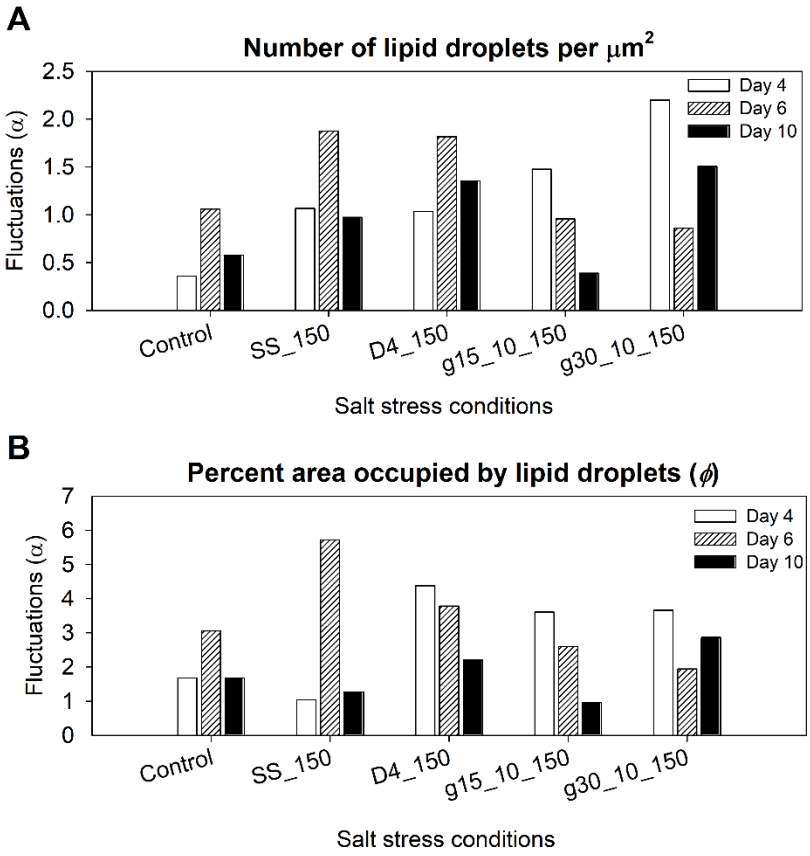

Figure 2.25. Fluctuations in the droplet growth dynamic properties in *C. reinhardtii* under the presence of 150 mM NaCl.

Fluctuations (α) in the number of lipid droplets (**A**) and the percentage area occupied by lipid droplets per cell, φ (**B**), as a function of culture growth condition and age. Here $\alpha = v/x^2$ where α is the fluctuation in the measured variable, v is the variance in the data, and x is the mean of the variable.

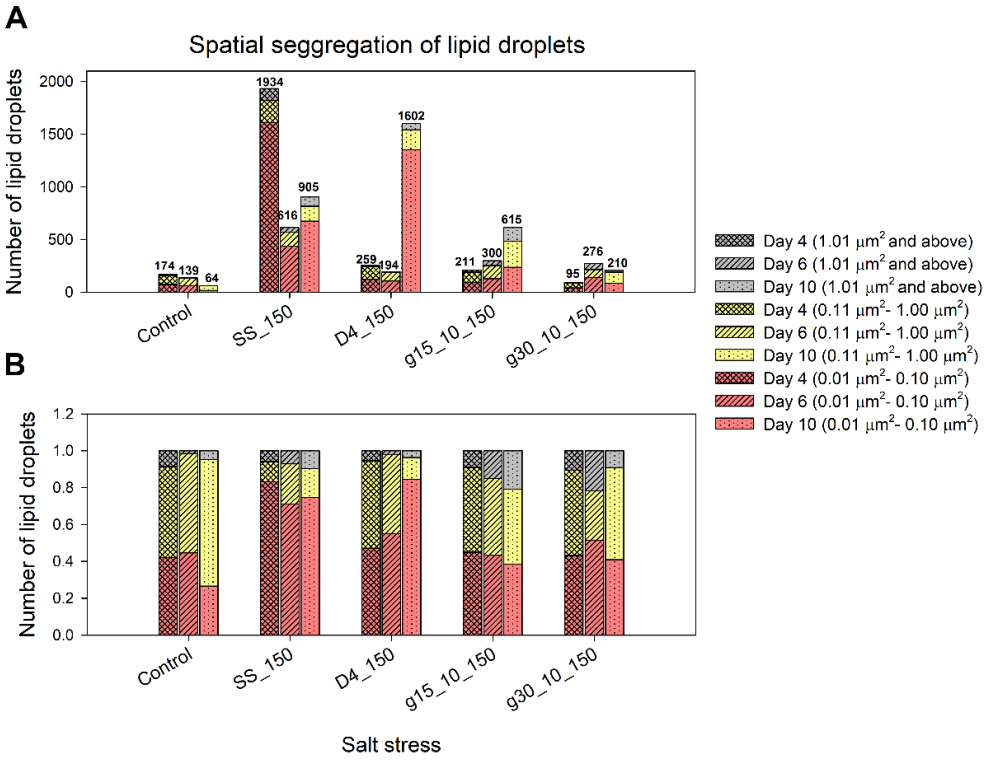

Figure 2.26. Spatial segregation of lipid droplets in the *C. reinhardtii* cells observed under the presence of 150 mM NaCl.

A. Average number of lipid droplets per cell for different growth conditions, with each bar representing the culture age, for a particular growth condition. **B**. Normalized bar plot representation of the number of droplets to show the fraction of each of the three categories of droplets in a cell for a given growth condition and culture age. The cross-checked bars represent day 4, bars with slants represent day 6 and dotted bars represent day 10. The droplets are subdivided into three categories based on their size - the largest droplets (1.01 μm^2 and above) are represented by gray-colored bars, the intermediate-sized droplets (0.11 μm^2 – 1.00 μm^2) are shown in yellow color, and the smallest droplets (0.01 μm^2 – 0.1 μm^2) are represented by the red shade.

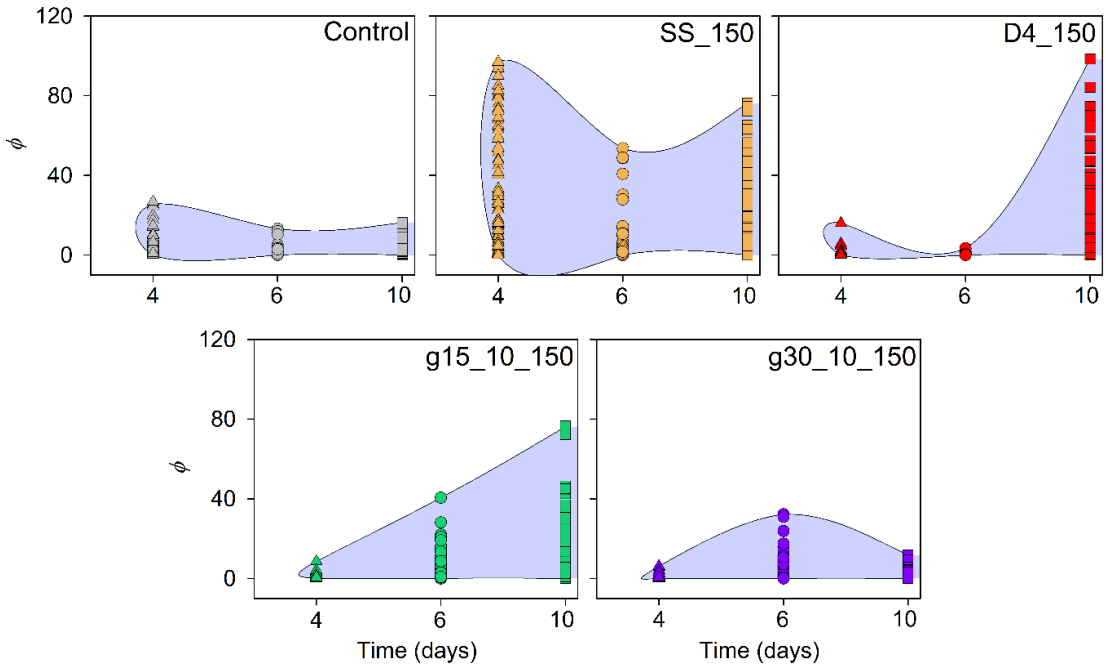

Figure 2.27. Liquid-liquid phase separation in lipid droplet biogenesis in *C. reinhardtii* under the presence of 150 mM NaCl.

Two-phase coexistence boundaries, with the blue region representing the lipid droplet's coexistence with the cytosol, for different growth conditions of *C. reinhardtii*. The fraction of area occupied by lipid droplets as a function of the age of the culture (φ) is plotted as a function of time in days.

2.5 Discussion

While salt stress has been extensively studied for improving biofuel production in microalgae, this study provides unique insights into the metabolic behavior of freshwater microalga, *C. reinhardtii* CC-125, at different salt concentrations and modes of cultivation implemented to improve the biofuel and nutraceutical applications. Salt stress beyond a threshold is often fatal to cell survival and sub-lethal effects on the growth and biomolecule accumulation is dose-dependent. While 100 mM NaCl caused no negative impact on the cell density, 200 mM NaCl served as the toxic concentration (**Figures 2.4 & 2.5**). We found that 150 mM NaCl was the ideal concentration to build an optimum cell density. Hounslow et al. (2021) have reported a 1.8-times decrease in the biomass accumulation in *C. reinhardtii* strain CC-4325 at 200 mM NaCl. Another study also claims that 200 mM induces cell death in *C. reinhardtii* strain CC-124 (Fan and Zheng, 2017). Among the NaCl ranging from 25 to 100 mM NaCl in *C. mexicana*, the highest biomass was observed at 25 mM NaCl (Salama et al., 2013). The marginal change in the viability of *C. reinhardtii* when the NaCl concentration varied between 50 to 150 mM was also observed in the other studies (Khona et al., 2016; Mastrobuoni et al., 2012). Changing the mode of cultivation often aids in an improvement in biomass productivity. In this context, the gradient strategy yielded the maximum biomass at 150 mM NaCl (g30_10_150 with a step size of 2 days boosts the cell density by ~1.5 times) and also rescued the cells from dying with 200 mM final concentration. The gradient strategy of adding 200 mM NaCl in steps of 2 days resulted in a similar ~1.5 times increase in biomass productivity despite a reduced growth rate in *C. reinhardtii,* cultivated under continuous illumination with the light intensity of 81 µmol photons m^{-2} s^{-1}, higher than the current study (Fal et al., 2022). The excess light intensity does not seem to change biomass productivity in gradient cultivation under salt stress.

Salt stress is a common practice to increase carotenoid production in microalgae (Benavente-Valdés et al., 2016; Bazzani et al., 2021). There is an increase in intracellular oxidative stress causing ROS production (Bazzani et al., 2021; Chokshi et al., 2017). Increased ROS levels induce autophagy and prolonged exposure leads to cell death (Affenzeller et al., 2009). To counter-regulate autophagy, carotenoid production increases (Ren et al., 2021). Annamalai et al. (2016) observed maximum production at the stationary phase in presence of 50 mM NaCl and the content gradually declined as the NaCl concentration increased to 300 mM in *C. reinhardtii* culture grown in bold

basal medium. In the present study, the chlorophyll and carotenoid content increased at 100 mM NaCl and then decreased with increasing NaCl concentration, when *C. reinhardtii* CC-125 was grown in a Tris-acetate phosphate medium (**Figure 2.6**). Thus, under constant cultivation environment conditions but with changing medium composition, the threshold level of salt tolerance in *C. reinhardtii* changes. Hang et al. (2020) found no significant change in chlorophyll concentration up to 100 mM as compared to the Control culture of axenic *C. reinhardtii*. The maximum chlorophyll content obtained from *Scenedesmus* sp. in presence of 170 mM NaCl was 25.03 ± 0.03 μg/ml chl *a* and 42.55 ± 0.63 μg/ml chl *b*. The carotenoid yield was 3.29 ± 0.005 mg/ml (Elloumi et al., 2020). *Chlorella vulgaris* produces a maximum of 15.29 ± 0.66 μg/ml of total chlorophyll and 1.74 ± 0.09 μg/ml of total carotenoid in presence of 30 mM NaCl (Yun et al., 2019). The present study offers the highest content of carotenoids and chlorophyll with 6.3 ± 0.64 mg/ml and 30.45 ± 3.6 mg/ml, respectively in presence of 100 mM NaCl applied in the single stage (**Figure 2.6**). The gradient addition of salt results in enhanced pigment accumulation but less than the Control, as also observed in a separate study conducted by Fal et al. (2022) in *C. reinhardtii*, exposed to gradient stress of 200 mM NaCl. They reported the production of 5.28 ± 0.5 mg/L chl *a*, 1.24 ± 0.2 mg/L chl *b*, and 2.6 ± 0.2 mg/L carotenoids which are significantly less than the content obtained in the present study. The increase in the light intensity and change in the growth medium to BG-11 are the likely causes of the reduction of pigment concentration (Fal et al., 2022). The decrease in pigment content due to salt toxicity is attributed to the altered PSII activity (Neelam and Subramanyam, 2013) and the hampered carbon-concentrating mechanism in microalgae (Hounslow et al., 2021). Salt stress-imposed oxidative imbalance also triggers chlorophyll degradation (Ji et al., 2018).

Salt toxicity induces excess production of starch and TAG. Starch molecules act as osmoprotectants and help the cells to adapt to osmotic stress induced by salt exposure (Tietel et al., 2020; Pandit et al., 2017). Lipids, especially neutral lipids are important for membrane integrity disturbed due to osmotic pressure caused by salt toxicity (Ji et al., 2018). Their production is separated on a time scale and the phenomenon is called starch-to-lipid switching (Kato et al., 2017; Zhang et al., 2018). Starch production begins early in the metabolic stage followed by the lipids that are synthesized at the later growth stages (Fal et al., 2022; Hang et al., 2020). In the current work, maximum

starch content is observed on day 4 and TAG content on day 6 onwards (**Figures 2.11 & 2.12**). 150 mM NaCl is the optimum concentration to yield the maximum of both starch and TAG. A study with single-stage cultivation of *C. reinhardtii* strain CC-4325 yields only a 1.66 times increment in the carbohydrate content in 200 mM NaCl (Hounslow et al., 2021). Even the gradient cultivation of *C. reinhardtii* with 200 mM NaCl increased the carbohydrate content by 1.72 times only (Fal et al., 2022). This study offers a maximum increase in starch content, 65 times higher than the Control, from the single-stage cultivation of *C. reinhardtii* strain CC-125 (**Figure 2.11**). Two-stage salinity stress enhances the starch content in *Scenedesmus* sp. marginally by only 3% and neutral lipids by 10% (Pancha et al., 2015). In *C. reinhardtii* (axenic culture, NIES-2235), 200 mM NaCl increases lipid production by 2 times (Hang et al., 2020). Lipids witness the highest change by 2.5 folds in *Scenedesmus* sp. containing 200 mM NaCl in the surroundings (Ji et al., 2018). In *Scenedesmus obtusus* XJ-15, two-stage salt stress causes an increase in lipid productivity by 1.8 folds and changes the fatty acid composition (Xia et al., 2013). A freshwater microalga, *Chlorella vulgaris*, can produce 2.45 times excess lipids even in the presence of 500 mM NaCl added in two-stage cultivation due to the tolerance to the oxidative stress induced at high salt concentrations (Yun et al., 2019). The current study shows maximum lipid accumulation in the gradient cultivation with 150 mM NaCl, which is nearly 2 times higher than the Control (**Figure 2.11**). The combination of low-salt concentration and gradient strategy helps in enhancing the lipid content in microalgae.

An increase in the levels of reactive oxygen species in the cell under salt toxicity results in enhanced autophagy (Affenzeller et al., 2009). Increased ATG8 levels accompanied by enhanced DGAT levels in light-stressed cultures of *C. reinhardtii* results in enhanced TAG accumulation (Chouhan et al., 2022). Autophagy increases lipid production in *Haematococcus lacustris* under salinity stress (Zharova et al., 2022). *De novo* production pathways like fatty acid biosynthesis and TAG synthesis further complement the higher levels of TAG in salt stress in microalgae (Atikij et al., 2019; Iwai et al., 2014; Rengel et al., 2018). An increase in the starch degradation activity is also known to increase the carbon flow toward lipid production and result in starch-to-lipid switching (Kato et al., 2021). We observed highly upregulated levels of both catabolic and anabolic pathways in the gradient strategy, i.e., *ATG4, ATG8, PhoA, ACC*, and *DGAT* representing autophagy, starch degradation, and *de novo* lipid synthesis,

respectively. These together contribute to the higher levels of observed TAG (**Figure 2.13**). In single-stage cultivation, the autophagy levels are low and the *de novo* pathway alone is responsible for the lipid content. Two-stage salt stress exhibits autophagy along with protein turnover. However, the downregulation of RPS6 is related to the activation of autophagy (Pérez-Pérez et al., 2017). This is the first study to display the varying effect of the mode of cultivation on metabolic pathways and metabolite production.

High salinity exerts morphological changes like palmelloid formation, flagellar resorption, and a decrease in cell size (Khona et al., 2016). In *C. reinhardtii*, palmelloid formation starts beyond 50 mM NaCl (Neelam and Subramanyam, 2013). Palmelloid protect the cells enclosed within the EPS matrix from further external damage (Shetty et al., 2019). This study, for the first time, provides a detailed analysis of changing cell morphology as a function of the mode of cultivation. Single-stage cultivation with both 100 and 150 mM NaCl exhibits palmelloid formation, otherwise insignificant or delayed in two-stage and gradient cultivations (**Figures 2.14 & 2.18**). 100 mM NaCl exerts 4-6 celled structures while 150 mM increases the strength to 8-celled structure in single-stage. On the contrary, only 2-4 celled structures were observed in *C. reinhardtii* strain GY-D55 containing a higher salt concentration of 300 mM (Zhang et al., 2022). Osmotic shock results in size reduction but intact circularity in the single-stage cells with 100 mM and 150 mM NaCl (**Figures 2.15 & 2.20**). The gradient cultivation, g30_10_150, with maximum cell density shows no noteworthy change in their cell size. Bimodal distribution appears in two-stage cultivations signifying the development of stress-combat strategies in the population. These sub-populations slowly grow and take over the existing cells in the population, giving way to evolution for survival (Altschuler and Wu, 2010; Lidstrom and Konopka, 2010).

The TAG molecules synthesized under stress are enclosed by a phospholipid monolayer when pinched off from the ER membrane (Walther et al., 2017). These form a droplet-like structure called lipid droplets (LD). The size of LD varies greatly among different species of microalgae, for instance, *Chlamydomonas* produces LDs of size ~1.5 μm and *Chlorella* produces LDs of > 2 μm (Lin et al., 2012). Assuming the droplets are completely circular, the average diameter of LDs produced in the two-stage 100 mM NaCl is 0.65 μm (D2_100) and 0.75 μm in single-stage 150 mM (SS_150). The size of LDs differs with the mode of cultivation and increases with the salt concentration

(**Figures 2.17 & 2.21**). The LD size is believed to be governed by the physical phenomena of Ostwald ripening or droplet coalescence (Walther et al., 2017; Georgieva et al., 2009). The presence of certain proteins like seipin in the outer layer of LDs and DGAT, involved in TAG synthesis, regulates the size of LD (Zoni et al., 2020). The major lipid droplet proteins (MLDP) present in the outer layer of droplets in *C. reinhardtii* and *Phaeodactylum tricornutum* has been revealed to regulate the droplet size without affecting their metabolism and composition (Moellering and Benning, 2010; Wang et al., 2017). The chain length of fatty acids and unsaturation content present in triacylglycerol also modulate the size of LDs (Son et al., 2022; Lange et al., 2021). Since the fatty acid composition is likely to change with the environmental condition (Moser, 2009; Yu et al., 2011), it is easy to establish that the growth dynamics vary under different modes of cultivation under salt stress. The degradation of LDs to release energy when required to carry out metabolic activities further decides the LD size, under which state the size and number of LDs become independent of the actual concentration of the neutral lipid molecules (Yu and Li, 2017). The gradient cultivation is the perfect epitome of this theory where the lipid content is high but the number of LDs is low (**Figures 2.11 & 2.26**). Lipid droplet biogenesis begins with initial phase separation or demixing in the ER membrane (Olzmann and Carvalho, 2019). The droplet formation by liquid-liquid phase separation (LLPS) theory can be described by generalizing the Flory-Huggins relation for free energy (Flory, 1954). In microalgae, LLPS plays a vital role in sensing oxidative stress and aids LD formation (Saito and Kimura, 2021). The presence of an increased two-phase state, explained by the function of area fraction of lipid droplet with culture age, in single-stage could be due to the reduced lipid concentration (**Figures 2.11 & 2.27**). The LD biogenesis differs among organelles. The nuclear LDs are different from the cytoplasmic ones (Fujimoto, 2022). The LD formation is believed to initiate from both ER and chloroplast in microalgae (Goold et al., 2015). The spatial differences and membrane bending energy barrier are likely to regulate the phase separation and initial LD size to a great extent (Zoni et al., 2021; Mahamid et al., 2019). These features of droplet biogenesis would vary under stress (Zoni et al., 2021), as a result of which the demixed state increases under salt stress (**Figure 2.27**). These unique characteristics of droplet formation under salt stress and varying modes of cultivation is the unique finding of this study, which can be explored in detail in the future.

Summarizing, this study deals with a multidimensional approach to understanding the dose-dependent behavior of *C. reinhardtii* strain CC-125 under salt stress (**Figure 2.28**). The effects have been monitored at physiological, morphological, biochemical, genetic as well as single-cell levels on different aspects of growth and production of lipids, starch, and photosynthetic pigments. Low NaCl concentration benefited pigment production. 150 mM NaCl is the optimum concentration of sodium chloride to produce increased cell density, starch, and lipids. Changing the mode of cultivation to gradient from single-stage salt application enhanced cell density and lipid production. The excessive production of lipids is regulated by the combined action of autophagy, *de novo* lipid synthesis, and starch-to-lipid switching mechanisms. Gradient strategy minimizes the negative effects of osmotic pressure on cellular morphology. It modulates the size as well as the chemical nature of the lipid droplets. The phase separation involved in lipid droplet formation increases under salt stress and varies with the mode of cultivation. It depends on the lipid concentration balanced by the synthetic and breakdown pathways. Hence, this study provides an understanding of the effects of salt under different modes of cultivation can prove advantageous for the productivity of different forms of biofuel as well as nutraceuticals.

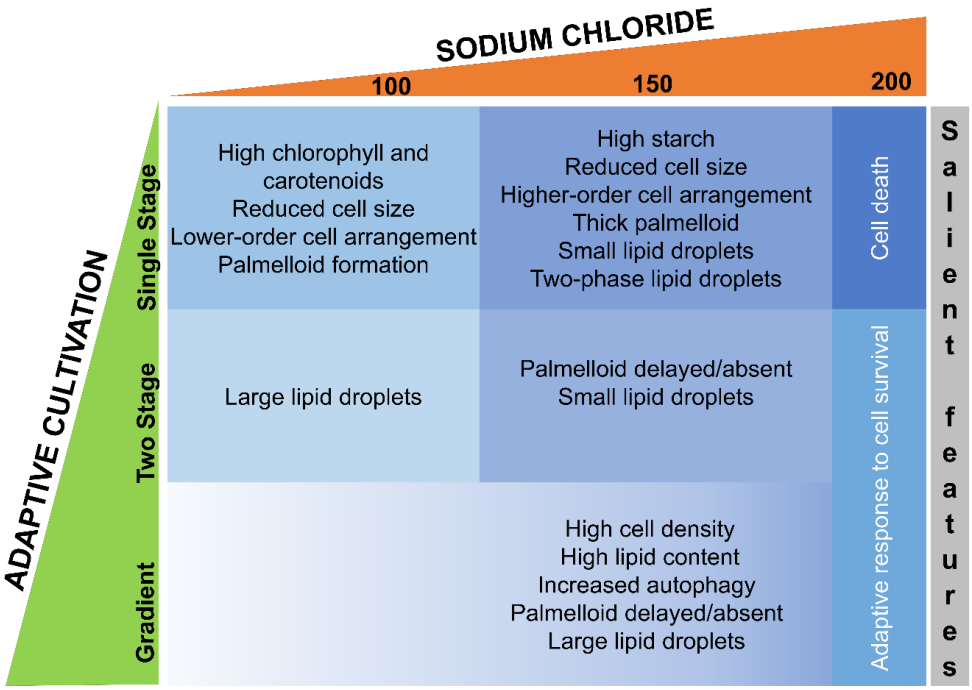

Figure 2.28. Summary of the salt stress-induced effects on the growth, morphology, and metabolite state of the *C. reinhardtii* cell.

2.6 Conclusion

The present study enlightens the relationship between the altering culture settings in presence of salt toxicity and the metabolic description of the microalgal cell. It signifies that the mode of cultivation is a key factor in diverting the metabolite production pathway from starch to lipid or vice versa. The benefits of the gradient method to increase cell count and lipid productivity will prove useful for larger-scale biodiesel production. The morphological changes inhabited by the microalgal cell under different culture environments are the unique findings of this study. The role of phase separation is essential in governing the oxidative imbalance of the cell and regulating the size of lipid droplets in the cytosol. This study reveals the changing properties of lipid droplets and phase separation with the culture age and the mode of cultivation under salt stress. Overall, this study presents an alternative approach with wide future perspectives in the field of salt stress-driven biofuel production in microalgae.

2.7 References

Affenzeller, M.J., A. Darehshouri, A. Andosch, C. Lütz, and U. Lütz-Meindl. 2009. Salt stress-induced cell death in the unicellular green alga *Micrasterias denticulata*. *J. Exp. Bot.* 60:939–954. doi:10.1093/jxb/ern348.

Altschuler, S.J., and L.F. Wu. 2010. Cellular Heterogeneity: Do Differences Make a Difference? *Cell*. 141:559–563. doi:10.1016/j.cell.2010.04.033.

Annamalai, J., J. Shanmugam, and T. Nallamuthu. 2016. Salt stress enhancing the production of Phytochemicals in *Chlorella vulgaris* and *Chlamydomonas reinhardtii*. *J. algal Biomass Util.* 7:37–44.

Atikij, T., Y. Syaputri, H. Iwahashi, T. Praneenararat, S. Sirisattha, H. Kageyama, and R. Waditee-Sirisattha. 2019. Enhanced lipid production and molecular dynamics under salinity stress in green microalga *Chlamydomonas reinhardtii* (137C). *Mar. Drugs*. 17. doi:10.3390/md17080484.

Bazzani, E., C. Lauritano, O. Mangoni, F. Bolinesi, and M. Saggiomo. 2021. *Chlamydomonas* responses to salinity stress and possible biotechnological exploitation. *J. Mar. Sci. Eng.* 9. doi:10.3390/jmse9111242.

Bell, S.A., C. Shen, A. Brown, and A.G. Hunt. 2016. Experimental Genome-Wide Determination of RNA Polyadenylation in *Chlamydomonas reinhardtii*. doi:10.1371/journal.pone.0146107.

Benavente-Valdés, J.R., C. Aguilar, J.C. Contreras-Esquivel, A. Méndez-Zavala, and J. Montañez. 2016. Strategies to enhance the production of photosynthetic pigments and lipids in chlorophycae species. *Biotechnol. Reports*. 10:117–125. doi:10.1016/j.btre.2016.04.001.

Black, S.K., S.L. Smolinski, C. Feehan, P.T. Pienkos, E.E. Jarvis, and L.M.L. Laurens. 2013. New method for discovery of starch phenotypes in growing microalgal colonies. *Anal. Biochem.* 432:71–73. doi:10.1016/j.ab.2012.09.018.

Chen, W., C. Zhang, L. Song, M. Sommerfeld, and Q. Hu. 2009. A high throughput Nile red method for quantitative measurement of neutral lipids in microalgae. *J. Microbiol. Methods*. 77:41–47. doi:10.1016/j.mimet.2009.01.001.

Chernomordik, L. V., and M.M. Kozlov. 2003. Protein-lipid interplay in fusion and fission of biological membranes. *Annu. Rev. Biochem.* 72:175–207. doi:10.1146/annurev.biochem.72.121801.161504.

Chokshi, K., I. Pancha, A. Ghosh, and S. Mishra. 2017. Salinity induced oxidative stress alters the physiological responses and improves the biofuel potential of green microalgae *Acutodesmus dimorphus*. *Bioresour. Technol.* 244:1376–1383. doi:10.1016/j.biortech.2017.05.003.

Chouhan, N., E. Devadasu, R.M. Yadav, and R. Subramanyam. 2022. Autophagy Induced Accumulation of Lipids in pgrl1 and pgr5 of *Chlamydomonas reinhardtii* Under High Light. *Front. Plant Sci.* 12. doi:10.3389/fpls.2021.752634.

Elloumi, W., A. Jebali, A. Maalej, M. Chamkha, and S. Sayadi. 2020. Effect of mild salinity stress on the growth, fatty acid and carotenoid compositions, and biological activities of the thermal freshwater microalgae *Scenedesmus* sp. *Biomolecules*. 10:1–17. doi:10.3390/biom10111515.

Fal, S., A. Aasfar, R. Rabie, A. Smouni, and H. EL Arroussi. 2022. Salt induced oxidative stress alters physiological, biochemical and metabolomic responses of green microalga

Chlamydomonas reinhardtii. *Heliyon*. 8. doi:10.1016/j.heliyon.2022.e08811.

Fan, J., and lvhong Zheng. 2017. Acclimation to NaCl and light stress of heterotrophic *Chlamydomonas reinhardtii* for lipid accumulation. *J. Biosci. Bioeng.* 124:302–308. doi:10.1016/j.jbiosc.2017.04.009.

Flory, P.J. 1954. Principles of Polymer Chemistry. Paul J. Flory. Cornell Univ. Press, Ithaca, New York, 1953. 688 pp. Illus. \$8.50. 119. 555–556 pp.

Fujimoto, T. 2022. Nuclear lipid droplets - how are they different from their cytoplasmic siblings? *J. Cell Sci.* 135. doi:10.1242/jcs.259253.

Georgieva, D., V. Schmitt, F. Leal-Calderon, and D. Langevin. 2009. On the possible role of surface elasticity in emulsion stability. *Langmuir*. 25:5565–5573. doi:10.1021/la804240e.

Goold, H., F. Beisson, G. Peltier, and Y. Li-Beisson. 2015. Microalgal lipid droplets: composition, diversity, biogenesis and functions. *Plant Cell Rep.* 34:545–555. doi:10.1007/s00299-014-1711-7.

Gour, R.S., V.K. Garlapati, and A. Kant. 2020. Effect of Salinity Stress on Lipid Accumulation in *Scenedesmus* sp. and *Chlorella* sp.: Feasibility of Stepwise Culturing. *Curr. Microbiol.* 77:779–785. doi:10.1007/s00284-019-01860-z.

Hang, L.T., K. Mori, Y. Tanaka, M. Morikawa, and T. Toyama. 2020. Enhanced lipid productivity of *Chlamydomonas reinhardtii* with combination of NaCl and CaCl2 stresses. *Bioprocess Biosyst. Eng.* 43:971–980. doi:10.1007/s00449-020-02293-w.

Ho, S.H., A. Nakanishi, Y. Kato, H. Yamasaki, J.S. Chang, N. Misawa, Y. Hirose, J. Minagawa, T. Hasunuma, and A. Kondo. 2017. Dynamic metabolic profiling together with transcription analysis reveals salinity-induced starch-To-lipid biosynthesis in alga *Chlamydomonas* sp. JSC4. *Sci. Rep.* 7:1–7. doi:10.1038/srep45471.

Ho, S.H., A. Nakanishi, X. Ye, J.S. Chang, K. Hara, T. Hasunuma, and A. Kondo. 2014. Optimizing biodiesel production in marine *Chlamydomonas* sp. JSC4 through metabolic profiling and an innovative salinity-gradient strategy. *Biotechnol. Biofuels*. 7:1–16. doi:10.1186/1754-6834-7-97.

Hounslow, E., C.A. Evans, J. Pandhal, T. Sydney, N. Couto, T.K. Pham, D.J. Gilmour, and P.C. Wright. 2021. Quantitative proteomic comparison of salt stress in *Chlamydomonas reinhardtii* and the snow alga *Chlamydomonas nivalis* reveals mechanisms for salt-triggered fatty acid accumulation via reallocation of carbon resources. *Biotechnol. Biofuels*. 14:1–25. doi:10.1186/s13068-021-01970-6.

Iwai, M., K. Ikeda, M. Shimojima, and H. Ohta. 2014. Enhancement of extraplastidic oil synthesis in *Chlamydomonas reinhardtii* using a type-2 diacylglycerol acyltransferase with a phosphorus starvation-inducible promoter. *Plant Biotechnol. J.* 12:808–819. doi:10.1111/pbi.12210.

Ji, X., J. Cheng, D. Gong, X. Zhao, Y. Qi, Y. Su, and W. Ma. 2018. The effect of NaCl stress on photosynthetic efficiency and lipid production in freshwater microalga-*Scenedesmus obliquus* XJ002. *Sci. Total Environ.* 633:593–599.

Johnson, X., and J. Alric. 2013. Central carbon metabolism and electron transport in *Chlamydomonas reinhardtii*: Metabolic constraints for carbon partitioning between oil and starch. *Eukaryot. Cell*. 12:776–793. doi:10.1128/EC.00318-12.

Kato, Y., S.H. Ho, C.J. Vavricka, J.S. Chang, T. Hasunuma, and A. Kondo. 2017. Evolutionary engineering of salt-resistant *Chlamydomonas* sp. strains reveals salinity stress-activated starch-to-lipid biosynthesis switching. *Bioresour. Technol.* 245:1484–1490.

doi:10.1016/j.biortech.2017.06.035.

Kato, Y., T. Oyama, K. Inokuma, C.J. Vavricka, M. Matsuda, R. Hidese, K. Satoh, Y. Oono, J.S. Chang, T. Hasunuma, and A. Kondo. 2021. Enhancing carbohydrate repartitioning into lipid and carotenoid by disruption of microalgae starch debranching enzyme. *Commun. Biol.* 4. doi:10.1038/s42003-021-01976-8.

Khan, M.U., and K. Mitchell. 1987. Chlorophylls Carotenoids. *Methods Enzymol.* 148:350–382.

Khona, D.K., S.M. Shirolikar, K.K. Gawde, E. Hom, M.A. Deodhar, and J.S. D'Souza. 2016. Characterization of salt stress-induced palmelloids in the green alga, *Chlamydomonas reinhardtii*. *Algal Res.* 16:434–448. doi:10.1016/j.algal.2016.03.035.

Kou, Z., S. Bei, J. Sun, and J. Pan. 2013. Fluorescent measurement of lipid content in the model organism *Chlamydomonas reinhardtii*. *J. Appl. Phycol.* 25:1633–1641. doi:10.1007/s10811-013-0011-x.

Lange, M., P.V. Wagner, and M. Fedorova. 2021. Lipid composition dictates the rate of lipid peroxidation in artificial lipid droplets. *Free Radic. Res.* 55:469–480. doi:10.1080/10715762.2021.1898603.

Li-Beisson, Y., F. Beisson, and W. Riekhof. 2015. Metabolism of acyl-lipids in *Chlamydomonas reinhardtii*. *Plant J.* 82:504–522. doi:10.1111/tpj.12787.

Lidstrom, M.E., and M.C. Konopka. 2010. The role of physiological heterogeneity in microbial population behavior. *Nat. Chem. Biol.* 6:705–712. doi:10.1038/nchembio.436.

Lin, I.P., P.L. Jiang, C.S. Chen, and J.T.C. Tzen. 2012. A unique caleosin serving as the major integral protein in oil bodies isolated from *Chlorella* sp. cells cultured with limited nitrogen. *Plant Physiol. Biochem.* 61:80–87. doi:10.1016/j.plaphy.2012.09.008.

Lv, H., G. Qu, X. Qi, L. Lu, C. Tian, and Y. Ma. 2013. Transcriptome analysis of *Chlamydomonas reinhardtii* during the process of lipid accumulation. *Genomics*. 101:229–237. doi:10.1016/j.ygeno.2013.01.004.

Mahamid, J., D. Tegunov, A. Maiser, J. Arnold, H. Leonhardt, J.M. Plitzko, and W. Baumeister. 2019. Liquid-crystalline phase transitions in lipid droplets are related to cellular states and specific organelle association. *Proc. Natl. Acad. Sci. U. S. A.* 116:16866–16871. doi:10.1073/pnas.1903642116.

Maneechote, W., and B. Cheirsilp. 2021. Stepwise-incremental physicochemical factors induced acclimation and tolerance in oleaginous microalgae to crucial outdoor stresses and improved properties as biodiesel feedstocks. *Bioresour. Technol.* 328:124850. doi:10.1016/j.biortech.2021.124850.

Mastrobuoni, G., S. Irgang, M. Pietzke, H.E. Aßmus, M. Wenzel, W.X. Schulze, and S. Kempa. 2012. Proteome dynamics and early salt stress response of the photosynthetic organism *Chlamydomonas reinhardtii*. *BMC Genomics*. 13:1–13. doi:10.1186/1471-2164-13-215.

Moellering, E.R., and C. Benning. 2010. RNA interference silencing of a major lipid droplet protein affects lipid droplet size in *Chlamydomonas reinhardtii*. *Eukaryot. Cell*. 9:97–106. doi:10.1128/EC.00203-09.

Moser, B.R. 2009. Biodiesel production, properties, and feedstocks. *Vitr. Cell. Dev. Biol. - Plant*. 45:229–266. doi:10.1007/s11627-009-9204-z.

Nagappan, S., S. Devendran, P.C. Tsai, H.U. Dahms, and V.K. Ponnusamy. 2019. Potential of two-stage cultivation in microalgae biofuel production. *Fuel*. 252:339–349. doi:10.1016/j.fuel.2019.04.138.

Neelam, S., and R. Subramanyam. 2013. Alteration of photochemistry and protein degradation of photosystem II from *Chlamydomonas reinhardtii* under high salt grown cells. *J. Photochem. Photobiol. B Biol.* 124:63–70. doi:10.1016/j.jphotobiol.2013.04.007.

Olzmann, J.A., and P. Carvalho. 2019. Dynamics and functions of lipid droplets. *Nat. Rev. Mol. Cell Biol.* 20:137–155. doi:10.1038/s41580-018-0085-z.

Pancha, I., K. Chokshi, R. Maurya, K. Trivedi, S.K. Patidar, A. Ghosh, and S. Mishra. 2015. Salinity induced oxidative stress enhanced biofuel production potential of microalgae *Scenedesmus* sp. CCNM 1077. *Bioresour. Technol.* 189:341–348. doi:10.1016/j.biortech.2015.04.017.

Pandit, P.R., M.H. Fulekar, and M.S.L. Karuna. 2017. Effect of salinity stress on growth, lipid productivity, fatty acid composition, and biodiesel properties in *Acutodesmus obliquus* and *Chlorella vulgaris*. *Environ. Sci. Pollut. Res.* 24:13437–13451. doi:10.1007/s11356-017-8875-y.

Pérez-Pérez, M., I. Couso, L. Heredia-Martínez, and J. Crespo. 2017. Monitoring Autophagy in the Model Green Microalga *Chlamydomonas reinhardtii*. *Cells*. 6:36. doi:10.3390/cells6040036.

Pérez-Pérez, M.E., I. Couso, and J.L. Crespo. 2012. Carotenoid deficiency triggers autophagy in the model green alga *Chlamydomonas reinhardtii*. *Autophagy*. 8:376–388. doi:10.4161/auto.8.3.18864.

Ren, Y., H. Sun, J. Deng, J. Huang, and F. Chen. 2021. Carotenoid production from microalgae: Biosynthesis, salinity responses and novel biotechnologies. *Mar. Drugs*. 19. doi:10.3390/md19120713.

Rengel, R., R.T. Smith, R.P. Haslam, O. Sayanova, M. Vila, and R. León. 2018. Overexpression of acetyl-CoA synthetase (ACS) enhances the biosynthesis of neutral lipids and starch in the green microalga *Chlamydomonas reinhardtii*. *Algal Res.* 31:183–193. doi:10.1016/j.algal.2018.02.009.

Saito, Y., and W. Kimura. 2021. Roles of Phase Separation for Cellular Redox Maintenance. *Front. Genet.* 12:1–15. doi:10.3389/fgene.2021.691946.

Salama, E.S., H.C. Kim, R.A.I. Abou-Shanab, M.K. Ji, Y.K. Oh, S.H. Kim, and B.H. Jeon. 2013. Biomass, lipid content, and fatty acid composition of freshwater *Chlamydomonas mexicana* and *Scenedesmus obliquus* grown under salt stress. *Bioprocess Biosyst. Eng.* 36:827–833. doi:10.1007/s00449-013-0919-1.

Shetty, P., M.M. Gitau, and G. Maróti. 2019. Salinity Stress Responses and Adaptation Mechanisms in Eukaryotic Green Microalgae. *Cells*. 8:1–16. doi:10.3390/cells8121657.

Son, S.H., G. Park, J. Lim, C.Y. Son, S.S. Oh, and J.Y. Lee. 2022. Chain flexibility of medicinal lipids determines their selective partitioning into lipid droplets. *Nat. Commun.* 13:1–11. doi:10.1038/s41467-022-31400-6.

Thiam, A.R., B. Antonny, J. Wang, J. Delacotte, F. Wilfling, T.C. Walther, R. Beck, J.E. Rothman, and F. Pincet. 2013. COPI buds 60-nm lipid droplets from reconstituted water-phospholipid- triacylglyceride interfaces, suggesting a tension clamp function. *Proc. Natl. Acad. Sci. U. S. A.* 110:13244–13249. doi:10.1073/pnas.1307685110.

Thiam, A.R., and L. Forêt. 2016. The physics of lipid droplet nucleation, growth and budding. *Biochim. Biophys. Acta - Mol. Cell Biol. Lipids*. 1861:715–722. doi:10.1016/j.bbalip.2016.04.018.

Tietel, Z., W.R. Wikoff, T. Kind, Y. Ma, and O. Fiehn. 2020. Hyperosmotic stress in

Chlamydomonas induces metabolomic changes in biosynthesis of complex lipids. *Eur. J. Phycol.* 55:11–29. doi:10.1080/09670262.2019.1637547.

Walther, T.C., J. Chung, and R. V. Farese. 2017. Lipid droplet biogenesis. *Annu. Rev. Cell Dev. Biol.* 33:491–510. doi:10.1146/annurev-cellbio-100616-060608.

Wang, X., T. Bin Hao, S. Balamurugan, W.D. Yang, J.S. Liu, H.P. Dong, and H.Y. Li. 2017. A lipid droplet-associated protein involved in lipid droplet biogenesis and triacylglycerol accumulation in the oleaginous microalga *Phaeodactylum tricornutum*. *Algal Res.* 26:215–224. doi:10.1016/j.algal.2017.07.028.

Xia, L., H. Ge, X. Zhou, D. Zhang, and C. Hu. 2013. Photoautotrophic outdoor two-stage cultivation for oleaginous microalgae *Scenedesmus obtusus* XJ-15. *Bioresour. Technol.* 144:261–267. doi:10.1016/j.biortech.2013.06.112.

Xie, Y., K. Lu, X. Zhao, R. Ma, J. Chen, and S.H. Ho. 2019. Manipulating Nutritional Conditions and Salinity-Gradient Stress for Enhanced Lutein Production in Marine Microalga *Chlamydomonas* sp. *Biotechnol. J.* 14:1–28. doi:10.1002/biot.201800380.

Yu, J., and P. Li. 2017. The size matters: regulation of lipid storage by lipid droplet dynamics. *Sci. China Life Sci.* 60:46–56. doi:10.1007/s11427-016-0322-x.

Yu, W., W. Ansari, N.G. Schoepp, M.J. Hannon, S.P. Mayfield, and M.D. Burkart. 2011. Modifications of the metabolic pathways of lipid and triacylglycerol production in microalgae. *Microb. Cell Fact.* 10:1–11.

Yun, C.J., K.O. Hwang, S.S. Han, and H.G. Ri. 2019. The effect of salinity stress on the biofuel production potential of freshwater microalgae *Chlorella vulgaris* YH703. *Biomass and Bioenergy*. 127:105277. doi:10.1016/j.biombioe.2019.105277.

Zhang, L., H. Pei, S. Chen, L. Jiang, Q. Hou, Z. Yang, and Z. Yu. 2018. Salinity-induced cellular cross-talk in carbon partitioning reveals starch-to-lipid biosynthesis switching in low-starch freshwater algae. *Bioresour. Technol.* 250:449–456. doi:10.1016/j.biortech.2017.11.067.

Zhang, L.Y., Z.T. Xing, L.Q. Chen, X.J. Zhang, and S.J. Fan. 2022. Comprehensive Time-Course Transcriptome and Co-expression Network Analyses Identify Salt Stress Responding Mechanisms in *Chlamydomonas reinhardtii* Strain GY-D55. *Front. Plant Sci.* 13:1–17. doi:10.3389/fpls.2022.828321.

Zhang, P., Z. Li, L. Lu, Y. Xiao, J. Liu, J. Guo, and F. Fang. 2017. Effects of stepwise nitrogen depletion on carotenoid content, fluorescence parameters and the cellular stoichiometry of *Chlorella vulgaris*. *Spectrochim. Acta - Part A Mol. Biomol. Spectrosc.* 181:30–38. doi:10.1016/j.saa.2017.03.022.

Zharova, D.A., A.N. Ivanova, I. V. Drozdova, A.I. Belyaeva, O.N. Boldina, O. V. Voitsekhovskaja, and E. V. Tyutereva. 2022. Role of Autophagy in *Haematococcus lacustris* Cell Growth under Salinity. *Plants*. 11:1–19. doi:10.3390/plants11020197.

Zoni, V., R. Khaddaj, P. Campomanes, A.R. Thiam, R. Schneiter, and S. Vanni. 2021. Pre-existing bilayer stresses modulate triglyceride accumulation in the er versus lipid droplets. *Elife*. 10:1–24. doi:10.7554/eLife.62886.

Zoni, V., R. Khaddaj, P. Campomanes, R. Thiam, R. Schneiter, and S. Vanni. 2020. Lipid Droplet Biogenesis is Driven by Liquid-Liquid Phase Separation. *SSRN Electron. J.* 1–30. doi:10.2139/ssrn.3526890.